Acta Pharmaceutica Sinica B 2026;16(1):352−370

Chinese Pharmaceutical Association
Institute of Materia Medica, Chinese Academy of Medical Sciences

Acta Pharmaceutica Sinica B

www.elsevier.com/locate/apsb
www.sciencedirect.com

ORIGINAL ARTICLE

Chinese medicine and intermittent fasting integration therapy attenuate diabetic vascular calcification *via* miR21-5p/Tpm1-mediated osteogenic differentiation of VSMCs

Wenting Wang[a,b,†], Yanfei Liu[c,d,†], Yiwen Li[e], Qian Xu[a], Mengmeng Zhu[a], Jing Cui[a], Yue Liu[a,d,*]

[a]*National Clinical Research Center for Chinese Medicine Cardiology, Xiyuan Hospital, Chinese Academy of Chinese Medical Sciences, Beijing 100091, China*
[b]*Department of Traditional Chinese Medicine, Peking Union Medical College Hospital, Chinese Academy of Medical Sciences and Peking Union Medical College, Beijing 100730, China*
[c]*The Second Department of Geriatrics, Xiyuan Hospital of China Academy of Chinese Medical Sciences, Beijing 100091, China*
[d]*Key Laboratory of Disease and Syndrome Integration Prevention and Treatment of Vascular Aging, Xiyuan Hospital of China Academy of Chinese Medical Sciences, Beijing 100091, China*
[e]*Beijing Key Laboratory of Traditional Chinese Medicine Basic Research on Prevention and Treatment for Major Diseases, Experimental Research Center, China Academy of Chinese Medical Sciences, Beijing 100007, China*

Received 30 January 2025; received in revised form 7 August 2025; accepted 26 August 2025

KEY WORDS

Vascular calcification;
Diabetes vascular complications;
Danlian-Tongmai formula;
Intermittent fasting;
Traditional Chinese medicine;
Dietary pattern

Abstract Vascular calcification (VC) is a marker of substantial vascular damage in patients with diabetes and has been recognized as a predictor of cardiovascular events and all-cause mortality. To date, no effective therapeutic strategy has been formulated for the management of VC. In this study, we integrated the treatment regimen of the Danlian-Tongmai (DLTM) formula, a traditional Chinese medicine (TCM) with anti-diabetic VC (anti-DVC) effects with intermittent fasting (IF), and established the Chinese medicine and intermittent fasting integration therapy (CMIT). CMIT synergistically enhanced the regulation of calcium-phosphorus homeostasis and vascular repair, and demonstrated significantly greater efficacy than DLTM or IF monotherapy in inhibiting calcium deposition and osteogenic differentiation both *in vivo* and *in vitro*. Transcriptomic sequencing revealed that the *miR21-5p/Tpm1* axis mediated the

*Corresponding author.
E-mail address: liuyueheart@hotmail.com (Yue Liu).
†These authors made equal contributions to this work.

Peer review under the responsibility of Chinese Pharmaceutical Association and Institute of Materia Medica, Chinese Academy of Medical Sciences.

https://doi.org/10.1016/j.apsb.2025.11.016

anti-calcification effect of CMIT. *MiR21-5p* promoted the overproliferation, migration, and osteogenic differentiation of vascular smooth muscle cells (VSMC) by negatively regulating *Tpm1*, while CMIT inhibited such processes. In conclusion, this study demonstrated that CMIT inhibited the osteogenic differentiation of VSMC and restored its contractile phenotype by inhibiting the activation of the *miR21-5p/Tpm1* axis, thus exerting a therapeutic effect on DVC. CMIT may be a promising approach for the treatment of DVC.

1. Introduction

Vascular calcification (VC) is a common vascular pathology in patients with diabetes mellitus (DM) and is characterized by abnormal calcium phosphate deposition and vessel wall disorders and poses a serious threat to human health. Previous studies have shown that diabetic VC (DVC) is an active process regulated by multiple genes. DM-induced metabolic disorders first promote the osteogenic differentiation of vascular smooth muscle cells (VSMCs) in the vessel wall and induce aberrant calcium phosphate accumulation, leading to vascular sclerosis, impaired vascular function, and increased cardiovascular risks[1]. As an intermediate state between DM and DM-induced damage to target organs, such as the heart and kidney, VC has been prioritized for cardiovascular 1.5-level screening and intervention in patients with DM[2]. However, to date, an effective therapeutic strategy to prevent or halt the progression of VC in DM is lacking.

Traditional Chinese medicine (TCM) practitioners have accumulated rich clinical experience over a long term of practice, especially in the field of metabolic and cardiovascular diseases. Based on the concept of "preventing disease progression after disease onset", TCM has demonstrated significant therapeutic advantages in preventing and treating early metabolic and vascular damage. The Danlian-Tongmai (DLTM) formula, which is composed of five TCM herbal medicines (*Salvia miltiorrhiza* Bunge., *Coptis chinensis* Franch., *Polygonum cuspidatum* Siebold & Zucc., *Prunus mume* (Siebold) Siebold & Zucc., and *Rhodiola crenulata* (Hook.f. & Thomson) H. *Ohba*), has been widely used in the clinical treatment of diabetic coronary heart disease and DVC. In a previous study, we identified 108 major compounds of DLTM, including ferulic acid, berberine, and resveratrol, through ultra-performance liquid chromatography. We found that DLTM significantly ameliorated VC in diabetic rats and exerted its therapeutic effects of attenuating aortic calcium salt deposition and alleviating vascular inflammatory injury[3].

Recently, medical nutrition therapy represented by dietary pattern interventions have played a key role in the management of DM and its complications[4]. Intermittent fasting (IF) is a dietary pattern that restricts calorie intake within a specific period, including alternate-day fasting, time-restricted fasting, and the 5:2 diet. Numerous clinical and preclinical studies have highlighted the potential of IF in improving the symptoms and cardiovascular risk factors in patients with diabetes, including modulating glucose-lipid metabolism disorders, improving insulin sensitivity, and attenuating atherosclerosis and vascular remodeling[5-8]. Recently, emerging evidence suggested that IF combined with a low-calorie herbal nutritional regimen may be effective in improving long-term DM remission rates, restoring pancreatic islet function, and ameliorating metabolic abnormalities by improving intestinal dysbiosis[9,10]. Another study found that IF combined with Shen-Ling-Bai-Zhu-San and prebiotics ameliorated glucose and lipid metabolism disorders as well as aberrant liver and kidney functions and restored the diversity of the intestinal flora in diabetic mice[11]. In addition, considering the high drug burden of patients with diabetes, the combined dietary pattern can not only enhance the effect of drug therapy but also synergistically reduce the risk of cardiovascular events, serving as a comprehensive management strategy for patients with diabetes with a high risk of vascular complications. Therefore, this study aimed to integrate TCM and dietary therapy to establish a drug−food integration intervention strategy combining DLTM and IF (Chinese medicine and intermittent fasting integration therapy (CMIT)), assess the effectiveness of CMIT in the treatment of DVC, and explore its synergistic mechanisms by constructing a rat model of DVC and an in-vitro calcification model of VSMC.

2. Material and methods

2.1. Animal experiments

Six-week-old specific-pathogen-free (SPF)-grade male Sprague−Dawley (SD) rats were purchased from SiPeiFu (Beijing) Biotechnology Co., Ltd. SCXK (Beijing 2019-0010). All rats were housed in cages (five to six rats per cage) in a SPF-grade animal facility (with sterilized water and feed) at a temperature of 22 ± 2 °C, a humidity of 55 ± 5%, and a 12 h/12 h light cycle.

To model DVC, 30 mg/kg of streptozotocin (STZ) was injected intraperitoneally into the rats for 3 days to induce DM, and achieving fasting blood glucose >11.1 mmol/L was considered a successful modeling of DM[12]. After the blood glucose level was stabilized for 1 week, VC was induced by intraperitoneal injection of high-dose vitamin D3 (5.5×10^5 IU/kg) for 4 days as described in the literature[3].

To specifically overexpress *miR21-5p* in rats, a recombinant adeno-associated virus (AAV) serotype 8 gene transfer vector carrying shRNA and rno-*miR21-5p* sequences under the U6 promoter was constructed and administered *via* lateral tail vein injection. Ultimately, the packaged viral constructs were designated as *miR21-5p* OE (overexpression) and *miR21-5p* NC (negative control). Similarly, to specifically knock down *Tpm1* in rat VSMCs, we constructed a recombinant AAV serotype 8 gene transfer vector that carries shRNA targeting *Tpm1* sequences, driven by the *Sm22α* gene promoter to ensure specific manipulation of VSMCs. This vector was then administered *via* lateral tail vein injection. The packaged viral constructs were designated as *Tpm1* KD (knockdown) and *Tpm1* NC (negative control). The enhanced green fluorescent protein incorporated in the vector

served as a visual marker to verify viral transfection efficiency and monitor target sequence expression. The injection dose for each rat was 5×10^{11} gene copies/mL[13], with an injection volume of 0.1 mL. The animal experiments were conducted according to the animal ethical standards and were approved by the Animal Ethics Committee of Xiyuan Hospital, China Academy of Chinese Medical Sciences (approval No.: 2024XLC014-2), and adhered to the National Institutes of Health guidelines for the care and use of laboratory animals (NIH Publication No. 85-23, revised 1996).

2.2. Drug and dietary administration

The Chinese herbal tablets and the DLTM extract powder used in the study were identified and processed by the Institute of Chinese Meteria Medica, China Academy of Chinese Medical Sciences. A previous study by our research team was consulted for the preparation method and drug composition[3]. One gram of the DLTM extract powder contained 23.5 g of raw herbs, and the drug solution was freshly prepared with purified water immediately before use. The optimal dose (0.96 g/kg/day) identified in the previous study was used for oral gavage.

For IF, the 16:8 time-restricted fasting pattern was adopted[14]. The start of light exposure (8 am) was defined as ZT0, and the end of light exposure (8 pm) was defined as ZT12. The rats were allowed to eat for 8 h from 10 pm (ZT14) to 6 am (ZT22), and the feed was withdrawn until 10 pm on the second day. Only food intake was restricted throughout the fasting period, while water intake was not restricted.

2.3. In vivo identification of DLTM prototype compounds

SPF male SD rats ($n = 8$; 6-weeks-old, 200 ± 20 g) were purchased from SiPeiFu (Beijing) Biotechnology Co., Ltd. (SCXK (Beijing) 2019-0010) and randomly divided into two groups ($n = 4$ per group): a normal control group and a normal control + DLTM treatment group. The DLTM group was administered DLTM at 0.96 g/kg, a dose approximately four times the clinical daily dosage for DVC patients, while the control group received an equivalent volume of water. Blood samples (approximately 0.25 mL) were collected from the retinal venous plexus into EDTA-K2 anticoagulant tubes immediately before DLTM administration and at 0, 0.5, 1, 2, 4, 6, 8, 12, 14, 16, 18, 24, 36, and 48 h afterward. After centrifugation at 12,000 rpm (MR 23i Centrifuge, Thermo scientific, MA, USA) for 15 min, the resulting plasma was stored at −20 °C. All samples were pooled *via* the AUC method and deproteinated with 0.1% formic acid in methanol (*v/v*). Following vortex mixing and centrifugation (12,000 rpm, 10 min, 4 °C), the supernatant was dried under nitrogen, reconstituted in 100 μL of 50% methanol (*v/v*), and sonicated (40 kHz) for 30 min. The mixture was then centrifuged again at 12,000 rpm (MR 23i Centrifuge, Thermo scientific) for 10 min, and 1.0 μL of the final supernatant was injected into a UPLC−Q-TOF−MS/MS system for analysis. The HPLC−Q-TOF−MS/MS settings were as our previous study[3].

2.4. Cell lines and cultures

Human aortic vascular smooth muscle cells (HAVSMCs) were purchased from Hunan Fenghui Biotechnology Co., Ltd. (Cat. No. CL0115) and cultured in Dulbecco's modified Eagle's medium containing 10% fetal bovine serum (Solarbio, Beijing, China) and 1% double-antibody. To induce VSMC calcification, 30 mmol/L of glucose (Glu, Solarbio, Beijing, China), 10 mmol/L β-glycerophosphate (β-GP, Sigma), and 3 mmol/L calcium chloride ($CaCl_2$, Sigma) were added to the medium, followed by incubation for 7 days[15]. The medium was replaced every 2 days.

An *miR21-5p* mimic, *miR21-5p* inhibitor, and the corresponding NC (RiboBio, China, Guangzhou) were transfected into cells using Lipofectamine 2000 per the manufacturer's instructions. *Tpm1* siRNA and control siRNA (Sangon Biotech, China, Shanghai) were transfected into VSMC at a cell confluency of 60%−70% using Lipofectamine 2000. The corresponding sequence information is listed in Supporting Information Table S1.

2.5. Human peripheral blood mononuclear cells (PBMC) and aorta samples

Peripheral blood samples were obtained from outpatients and inpatients with Type 2 Diabetes Mellitus (T2DM) at the Department of Cardiovascular Medicine, Xiyuan Hospital, China Academy of Chinese Medical Sciences from March 2023 to March 2024. A total of 18 patients with T2DM with coronary artery calcification (CAC) and 10 patients with T2DM without CAC were recruited for this study. PBMCs were extracted from the peripheral blood using Ficoll-Hypaque (Solarbio, Beijing, China) gradient centrifugation. The extracted mixture was centrifuged at 800 rpm for 20 min (MR 23i Centrifuge, Thermo scientific), and the interface was collected as PBMCs. Clinical and biochemical parameters were collected from the patient's electronic medical records in the hospital. The study was conducted in accordance with the guidelines of the Declaration of Helsinki and was approved by Xiyuan Hospital, CACMS (2023XLA027-2). All patients provided informed consent before participating in the study.

Aortic samples were collected from six individuals, including three patients with T2DM complicated by CAC who underwent coronary artery bypass grafting at Peking University Third Hospital (Beijing, China), and three control subjects without diabetes or any clinical history of cardiovascular or metabolic diseases, with tissues obtained from a forensic institute, between April and October 2023. Clinical parameters were obtained from the hospital's electronic medical records. Aortic calcification was diagnosed using computed tomography and a definite Agatston score of >0. The clinical procedure was conducted according to the guidelines of the Declaration of Helsinki and was approved by the institutional review board of Peking University Third Hospital (2023 Medical Ethics Review No. (145-02)). All patients and their families provided informed consent before participating in the study.

2.6. Transcriptome RNA sequencing

Total RNA was isolated from fresh rat aorta using Trizol. Library construction and sequencing were performed by Beijing CapitalBio Technology Co., Ltd. Briefly, poly A-containing mRNA was purified using poly T oligonucleotide-attached magnetic beads. The mRNA was then cleaved into small fragments, followed by complementary DNA synthesis. The cDNA products were purified and amplified by polymerase chain reaction (PCR) to create the final cDNA library. Clusters were generated using cBot, and the libraries were diluted to 10 pmol/L before being sequenced using an Illumina NovaSeq 6000 (Illumina, CA, USA). A P-value of <0.05 and an FC ≥ 1.2 were used as the thresholds for identifying significantly differentially expressed genes (DEGs). Gene Ontology (GO) pathway enrichment analysis of

DEGs and the corresponding graphs were made using the clusterProfiler R package[16]. Protein−protein interaction (PPI) networks of DEGs were constructed using the STRING database[17], which were visualized using Cytoscape 3.9. Raw data from Transcriptome RNA Sequencing has been deposited at China National Genomics Data Center. Accession number: PRJCA035668.

2.7. Histopathology and immunofluorescence

Fresh rat aortic arches were fixed with 4% paraformaldehyde (PFA). Aortic arches were embedded in paraffin and serially sectioned from the proximal end at a thickness of 5 μm. For vascular histological analysis, three independent aortic sections were selected every 100 μm for each sample.

For alizarin red S staining, the aorta fixed with 4% PFA was immersed in 2% alizarin red S staining solution (Servicebio, China) overnight at 26 °C. The aorta was rinsed with 2% potassium hydroxide solution and photographed with an inverted microscope. For aortic arch sections, paraffin-embedded sections were dewaxed and stained with 1% alizarin red S solution for 5 min. After dehydration and fixation, the sections were observed under a digital microscope, and images were taken. VSMCs were rinsed thrice with phosphate buffer saline and fixed in 4% PFA for 15 min. After rinsing with PBS, VSMCs were stained with 1% alizarin red S solution (Servicebio, China) for 15 min.

For Von Kossa staining, paraffin-embedded aortic arch sections were dewaxed before 5% silver nitrate solution was added dropwise, followed by irradiation with ultraviolet light for 30 min, and rinsed thrice with distilled water. Thereafter, 5% sodium thiosulfate was added for 5 min to neutralize the unreacted silver. After rinsing thrice with distilled water, 0.1% nuclear fast red was added to restain the cell nucleus for 2 min. The sections were dehydrated and fixed, and images were taken using a digital microscope.

For the immunofluorescence experiment, 5-μm sections of human or rat aorta were dewaxed and rehydrated. Heat-mediated antigen retrieval was performed using a 10% citrate buffer. After the samples were incubated overnight with primary antibodies (anti-αSMA, anti-Tpm1), secondary antibodies were added dropwise and incubated for 60 min. Finally, coverslips were fixed in a fixation medium containing diamidino phenylindole (DAPI) (Abcam, UK). Images were obtained using a digital microscope.

2.8. Alkaline phosphatase (ALP) activity

Aortic tissue was lysed with inhibitor-free radio immunoprecipitating assay lysis buffer (Beyotime, China). ALP activity in the supernatant was measured using an ALP assay kit (Beyotime, China). The total protein content of the supernatant was determined by using the bicinchoninic acid method, and ALP activity (U/g protein) was standardized by dividing it by the protein content.

2.9. Calcium content detection

VSMCs and aortic tissues were lysed with inhibitor-free radio immunoprecipitating assay lysis buffer (Beyotime, China). Calcium content in the supernatant was measured using a calcium assay kit (Beyotime, China). The total protein content of the supernatant was determined by using the bicinchoninic acid method, and the calcium content was standardized by dividing it by the protein content (U/g protein).

2.10. Quantitative real-time PCR

Total RNA was extracted from aortic tissues and VSMCs using the Trizol reagent (Servicebio, China) per the manufacturer's instructions. The concentration of extracted RNA was measured using a spectrophotometer (NanoDrop, Thermo Fisher Scientific, USA). RNA was reverse transcribed into cDNA using a PrimeScript RT kit (Vazyme, China). The cDNA obtained was amplified *via* PCR using SYBR Green (Vazyme, China). Relative mRNA expression levels were analyzed using the $2^{-\Delta\Delta Ct}$ method with β-actin or U6. Primer sequences specific to the target genes are listed in Supporting Information Table S2.

2.11. Western blot (WB) analysis

Proteins were extracted from VSMCs and aortic tissues by using the RIPA lysis buffer (Beyotime, China) supplemented with the complete protease inhibitor mix (Beyotime, China), and the proteins were boiled for 10 min at 100 °C in the loading buffer (Beyotime, China). Equal amounts of proteins were separated on sodium dodecyl sulfate-polyacrylamide gels and transferred to polyvinylidene fluoride membranes (Millipore, Germany), which were incubated with primary antibodies at 4 °C overnight. On the next day, the membrane was incubated with an appropriate horse radish peroxidase-conjugated secondary antibody for 1 h at room temperature. Antibody binding was determined using the electrochemiluminescence assay (Millipore, Germany). Relative quantification of immune staining intensity was performed by grayscale analysis in ImageJ. The antibodies used in this study are listed in Supporting Information Table S3.

2.12. Statistical analysis

Statistical analysis and data visualization were performed using IBM SPSS Statistics (V26.0), Graphpad Prism (V9.5.0), and ImageJ. All data were expressed as mean ± standard error. For normally distributed data, one-way analysis of variance and Dunnett's test were performed for comparison between two or more groups. For non-normally distributed data, the Kruskal−Wallis test was performed. A $P < 0.05$ indicated that the differences were statistically significant. The VC Agatston score was a non-standardized parameter, and the logarithmic transformation of the Agatston score was used in the correlation analysis (Pearson correlation analysis). A $P < 0.05$ suggested that the difference was statistically significant.

3. Results

3.1. CMIT inhibited the formation of DVC

To comprehensively assess the effects of CMIT on DVC and determine the synergistic effects of DLTM and IF in ameliorating DVC, the effects of three treatment methods, namely, DLTM, IF, and CMIT, were compared (Fig. 1A). After modeling, the rats with DVC were randomly divided into four groups, namely the model group (DVC group), the group receiving DLTM (DLTM group), the group receiving IF (IF group), and the group receiving CMIT (CMIT group). A blank group was established using SD rats (CON group). As expected, STZ combined with excessive calcium led to a significant increase in blood glucose levels, weight loss, and elevated serum calcium and ALP levels in rats.

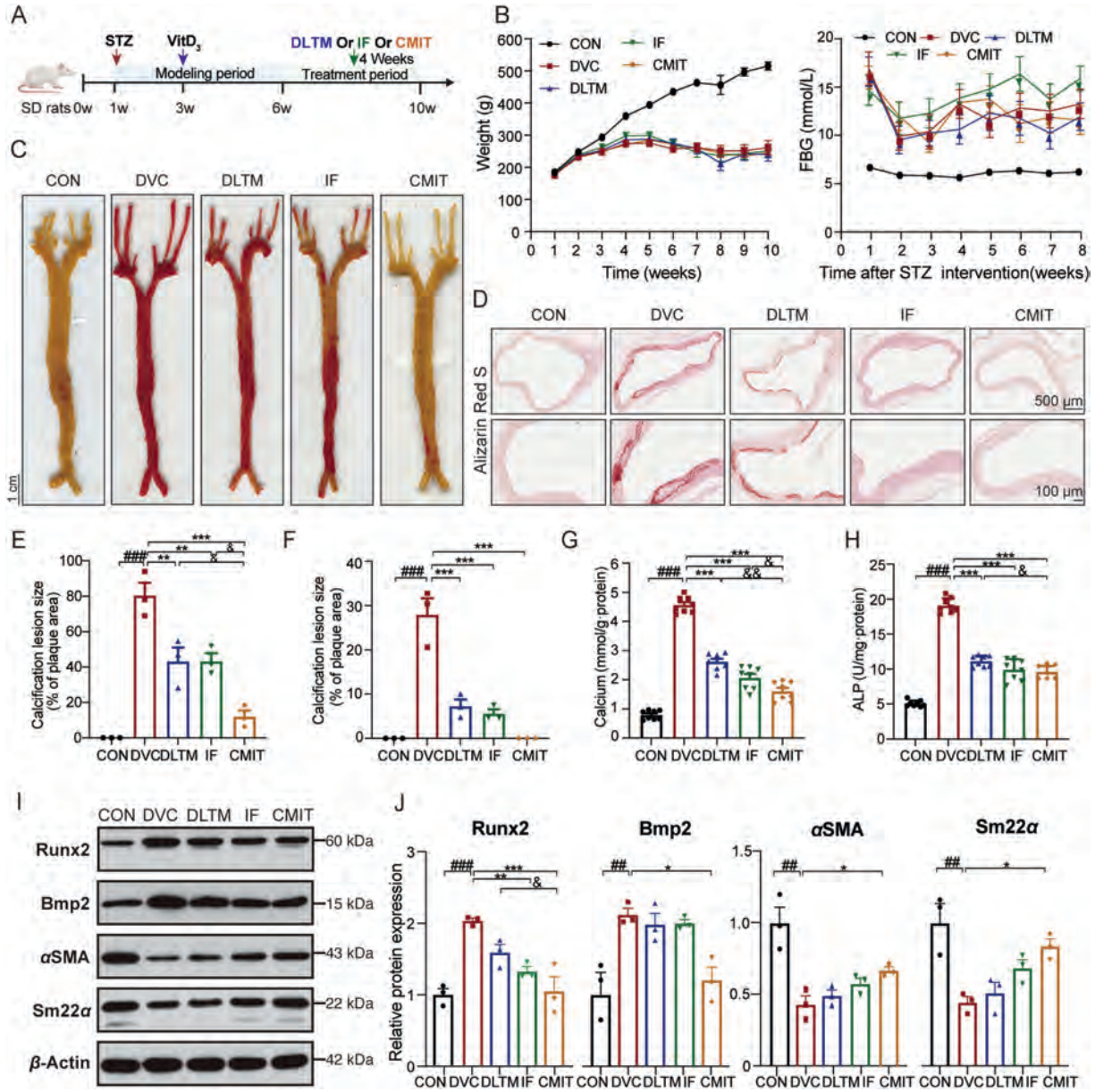

Figure 1 DLTM, in combination with IF, synergizes against DVC. (A) Flow chart of the animal experiment. Combination of STZ and vitamin D3 was used to construct a rat model of DVC, and the therapeutic effects of the three interventions, namely DLTM, IF, and CMIT, were observed; (B) Left: changes in the body weight of rats in each group during the experimental period ($n = 12$); Right: changes in fasting blood glucose levels of rats in each group during the experimental period ($n = 12$); (C) Representative images of alizarin-red staining of the aorta of rats in each group ($n = 3$); (D) Representative images of alizarin-red staining of the aorta arch of rats in each group ($n = 3, 4 \times , 10 \times$); (E) Quantitative alizarin-red staining of the entire aorta of rats in each group ($n = 3$); (F) Quantitative alizarin-red staining of the aorta arch of rats in each group ($n = 3$); (G) Calcium content in the aorta of rats in each group ($n = 8$); (H) ALP activity in the aorta of rats in each group ($n = 7-8$); (I) Representative WB images of Runx2, Bmp2, αSMA, and Sm22α expressions ($n = 3$) in the aorta of rats in each group; (J) Quantitative analysis of Runx2, Bmp2, αSMA, and Sm22α expressions in I ($n = 3$). FBG: fasting blood glucose. Data are expressed as mean ± SEM. Compared with the CON group, $^{\#\#\#}P < 0.001$; compared with the DVC group, $^{*}P < 0.05$, $^{**}P < 0.01$, $^{***}P < 0.001$; compared with the CMIT group, $^{\&}P < 0.05$, $^{\&\&\&}P < 0.001$.

DLTM, IF, and CMIT treatments resulted in limited improvement in blood glucose levels and body weight (Fig. 1B and Supporting Information Fig. S1A and S1B). However, serum calcium and ALP levels were influenced to varying degrees in the rats. Among the treatment methods, CMIT significantly reduced serum calcium and ALP levels in rats compared with DVC, and the effect was significantly better than that of DLTM and IF (Fig. S1C−S1E). In addition, the food intake of rats in the IF and CMIT groups was significantly reduced after fasting; however, no significant difference in food intake in each group throughout the experimental cycle was observed (Fig. S1F and S1G). Subsequently, the aortic calcification of rats in each group was observed. Compared with

the CON group, extensive calcified nodules and calcium salt deposits were observed in the entire aorta and the aortic arch of rats in the DVC group, and the lesions were mainly seen in tunica media and intima (Fig. 1C−F and Fig. S1H and S1I). Compared with the DVC group, the level of aortic calcification was reduced in the DLTM, IF, and CMIT groups sequentially. It should be noted that the aortic calcification in the CMIT group was the least severe and was significantly lower than that in the DLTM and IF groups (Fig. 1C−F and Fig. S1H and S1I). Similarly, the calcium content and ALP activity in the aortic tissues of rats in the DVC group were significantly higher than those in the CON group, confirming that the calcium deposition in the DVC group was more severe (Fig. 1G and H). Compared with the DVC group, the aortic calcium content and ALP activity of rats in the DLTM, IF, and CMIT groups decreased in that order. Moreover, the vascular calcium content of the CMIT group was significantly lower than that of the DLTM and IF groups, and the ALP activity of the CMIT group was significantly lower than that of the DLTM group (Fig. 1G and H). These findings indicated that the anti-VC effect of DLTM and IF was significantly enhanced when combined.

Osteogenic differentiation of VSMC plays a crucial role in VC. Hence, the effects of these three treatments on the osteogenic differentiation of VSMC were explored. Compared with the CON group, the *in vivo* expressions of osteogenic markers Bmp2 and Runx2 were significantly increased in the aorta of rats in the DVC group. In contrast, the expressions of contractile proteins αSMA and Sm22α decreased (Fig. 1I and J). No significant changes in contractile and osteogenic proteins were seen in the DLTM group compared with the DVC group. However, the expression of Runx2 was relatively decreased in the IF group; however, no significant change was seen in Bmp2 and contractile proteins. Significant decreases in the expressions of osteogenic proteins Runx2 and Bmp2, as well as significant increases in the expressions of contractile proteins αSMA and Sm22α, were observed only in rats in the CMIT group (Fig. 1I and J), which indicated that CMIT inhibited the osteogenic differentiation of VSMC *in vivo*. In conclusion, these data suggested that the CMIT strategy of combining TCM and diet was effective in inhibiting DVC and that the efficacy was significantly better than that of DLTM and IF monotherapies.

Next, to further clarify the role of CMIT on VSMC calcification *in vitro*, we first tracked the prototype compounds of DLTM (*i.e.*, the chemical constituents observed in both DLTM and plasma) to identify those with potential bioactivity against VC. Combining previous mass spectrometry results, we identified a total of 31 prototype compounds (Supporting Information Table S4), among which 8 were confirmed to have anti-calcification effects, including salidroside[18], gallic acid[19], resveratrol[20], rosmarinic acid[21], rutin[22], luteolin[23], curcumin[24], and tanshinone IIA[25].

Subsequently, we constructed a high-glucose calcification model of VSMCs *in vitro*. VSMC calcification was assessed by Alizarin Red staining, cell viability, calcium content, and the expression of osteogenic and contractile proteins. VSMC was divided into ordinary medium group (NG group), high glucose medium group (HG group) and high glucose osteogenic medium group (HGCM group) (Supporting Information Fig. S2A). Consistent with the findings of previous studies, high glucose levels combined with osteogenic medium (high phosphorus and calcium levels) significantly promoted VSMC calcification, including significant increases in the intensity of alizarin red staining and calcium content, an elevation in the expressions of the osteogenic markers Bmp2 and Runx2, and a decrease in the expressions of contractile proteins αSMA and Sm22α (Fig. S2B−S2E).

Then, we simulated *in vitro* ischemic conditions with serum deprivation (IF) and observed the effects of these DLTM compounds on VSMC activity and calcium content with and without combined IF. We found that, compared to the NG group, VSMCs in the HGCM group exhibited a pronounced hyperproliferative phenotype, and all DLTM compounds and IF effectively inhibited VSMC proliferation (Supporting Information Fig. S3A). Notably, the combination of DLTM with IF significantly amplified the suppression of VSMC hyperproliferation compared to individual DLTM compounds (Fig. S3A).

In addition, compared to the NG group, the calcium content in HGCM group cells was significantly increased. IF intervention did not notably affect cellular calcium content, while most DLTM compounds effectively reduced cellular calcium levels. Importantly, compared to intervention with individual DLTM compounds, the combination with IF often further enhanced their calcium-lowering effects, particularly for resveratrol, rosmarinic acid, curcumin, and tanshinone IIA (Fig. S3B). Although some individual compounds did not exhibit significant synergistic effects following combined IF, overall, CMIT could more significantly inhibit VSMC phenotype transformation and calcification.

3.2. Tpm1 may be a potential target for the anti-DVC effects of CMIT

To elucidate the unique synergistic mechanism of CMIT for the treatment of DVC, the validation strategy involving the filtering of RNA sequencing was adopted. Transcriptome sequencing analysis showed significant changes in the aortic transcriptome profiles of rats in the DVC group, with a total of 494 DEGs filtered compared with the CON group. Among them, there were 137 upregulated genes and 357 downregulated genes. DLTM, IF, and CMIT treatments all had significant effects on the aortic transcriptomic profiles of rats (Fig. 2A and Supporting Information Fig. S4A). Analysis of intersecting DEGs revealed that the DEGs regulated in the CMIT group were the most abundant compared with those regulated in the DLTM and IF groups (Fig. 2A). Given the optimal effect of CMIT in ameliorating DVC, we hypothesized that the synergistic anti-VC mechanism of CMIT might be related to the 61 DEGs independently regulated by CMIT. GO enrichment analysis based on these DEGs showed enrichment in multiple biological processes related to cytoskeletal structure and contractile actions, such as cytoskeleton organization, cardiac muscle cell development, and regulation of heart contraction (Fig. 2B and Fig. S4B−S4D). The Kyoto Encyclopedia of Gene and Genomes pathway analysis showed that CMIT significantly affects the gene expressions of signaling pathways such as cardiac structure and muscle contraction (Fig. 2C and Fig. S4E). Among the top DEGs associated with calcification, special attention was paid to *Tpm1*, as it was enriched in multiple core pathways and demonstrated significant intergroup differences in its expressions (Fig. 2C−E, Fig. S4F). Previous studies have shown that *Tpm1* was closely related to VSMC status and phenotypic transformation and is involved in several important processes, such as cytoskeletal regulation, as well as skeletal and cardiac muscle contraction[26]. To understand the correlation between *Tpm1* and DVC, we assessed the expression levels of *Tpm1* in DVC and the effects of different interventions. As expected, the decrease in *Tpm1* expression induced by DVC was reversed by CMIT therapy at both

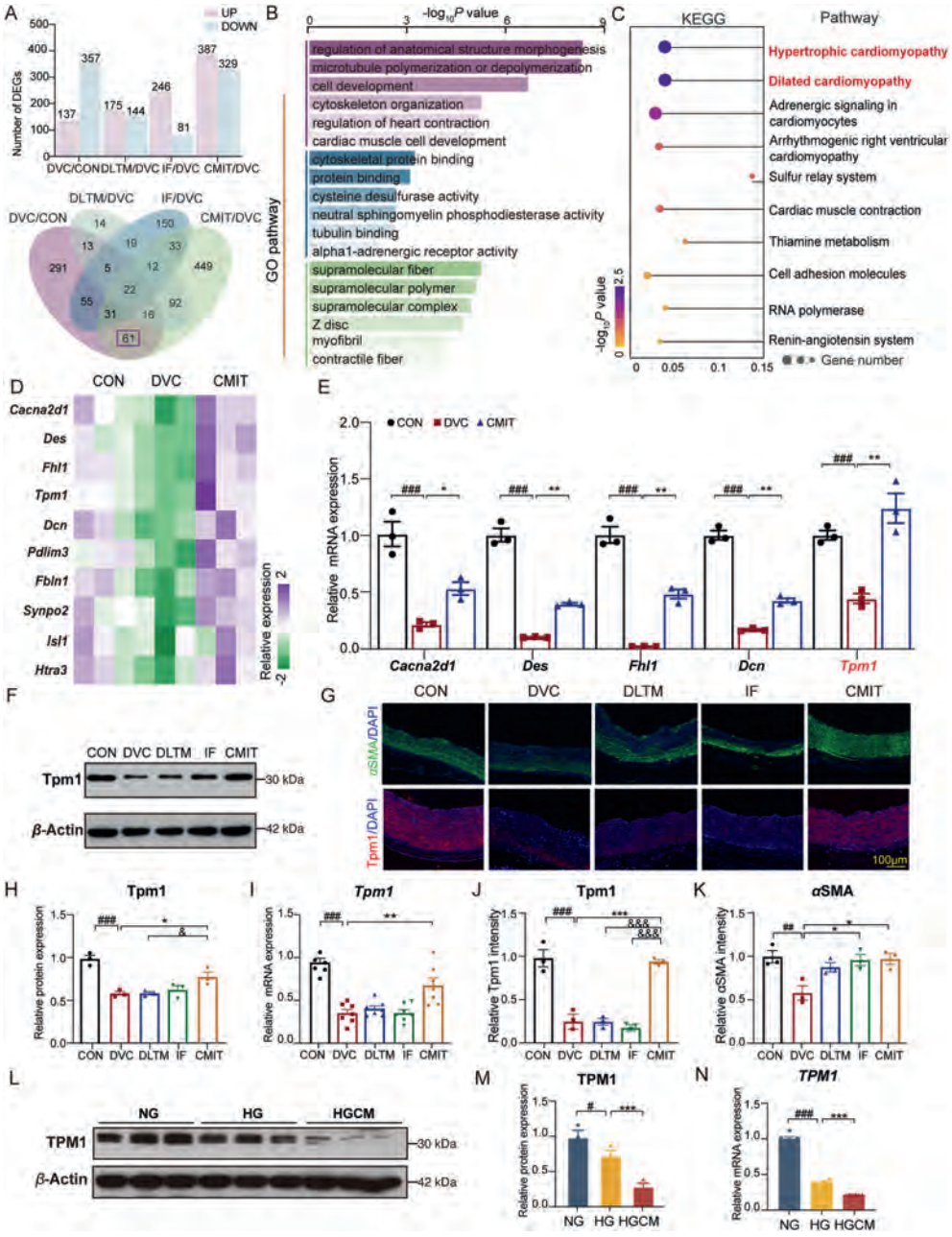

Figure 2 CMIT targets *Tpm1* in regulating DVC. (A) Upper panel: up- and downregulation of DEGs in each group compared. Lower panel: Venn diagram of DEGs in each group compared; (B) Bar graph of the top 15 enriched GO entries of DEGs; (C) Bubble chart of the top 10 enriched KEGG pathways of DEGs; (D) Heat map of the expression of the core targets in PPI between different groups; (E) PCR validation of the expressions of core targets in each group ($n = 3$); (F) Representative WB images of *Tpm1* expression in the rat aorta of each group ($n = 3$); (G) Representative images of immunofluorescence staining of *αSMA* (green) and *Tpm1* (red) in aortic sections of each group of rat, and the nuclei were re-stained with DAPI (blue) ($n = 3$, 20 ×); (H) Quantitative analysis of Tpm1 protein expression ($n = 3$, 20 ×); (I) *Tpm1* mRNA expression in the rat aorta in each group ($n = 7$); (J) Quantitative analysis of the fluorescence intensity of *Tpm1* in G ($n = 3$); (K) Quantitative analysis of the fluorescence intensity of *αSMA* in G ($n = 3$); (L) Representative WB images of Tpm1 expression in HAVSMC in each group ($n = 3$); (M) Quantitative analysis of Tpm1 expression in L ($n = 3$); (N) *Tpm1* mRNA expression in HAVSMC in each group ($n = 5$). GO: Gene Ontology, KEGG: Kyoto Encyclopedia of Genes and Genomes, DEG: differentially expressed genes. Data are expressed as mean ± SEM. Compared with the CON group or the NG group, $^{\#}P < 0.05$, $^{\#\#}P < 0.01$, $^{\#\#\#}P < 0.001$; compared with the DVC group or the HG group, $^{*}P < 0.05$, $^{**}P < 0.01$, $^{***}P < 0.001$; compared with the CMIT group, $^{\&}P < 0.05$, $^{\&\&}P < 0.01$.

transcriptional and protein levels, while DLTM and IF interventions had less effect on *Tpm1* (Fig. 2F–K). In addition, we also observed the expression levels of *Tpm1* in the high-glucose calcification model of VSMCs *in vitro*, the expressions of Tpm1 protein and mRNA gradually decreased with the increased calcification (Fig. 2L–N). These findings suggested that *Tpm1* was

involved in the osteogenic differentiation and calcification of VSMCs and that *Tpm1* may be a potential target of the anti-DVC effect of CMIT.

Given that *Tpm1* expression gradually decreases during diabetic VC and VSMC osteogenic differentiation, we next attempted to assess whether the knockdown of *Tpm1* would exacerbate VC in diabetic rats. We used recombinant AAV carrying scrambled shRNA (*Tpm1* NC) or *Tpm1* shRNA (*Tpm1* KD) to regulate *Tpm1* expression in VSMCs (Fig. 3A). Compared to the control group, the expression of *Tpm1* in the aorta of rats was significantly reduced after *Tpm1* knockdown (Fig. 3B and C). We then examined body weight, blood glucose levels, and the status of VC across different groups of rats. Consistent with previous results, compared with the CON group, the DVC and intervention groups showed significantly reduced body weight and elevated blood glucose levels (Supporting Information Fig. S5A−S5D). In addition, serum calcium, phosphate, and ALP levels were increased (Fig. S5E−S5G). However, no significant differences in these parameters were observed among the intervention groups (Fig. S5A−S5G).

At the same time, *Tpm1* knockdown significantly aggravated VC in diabetic rats, including promoting the deposition of

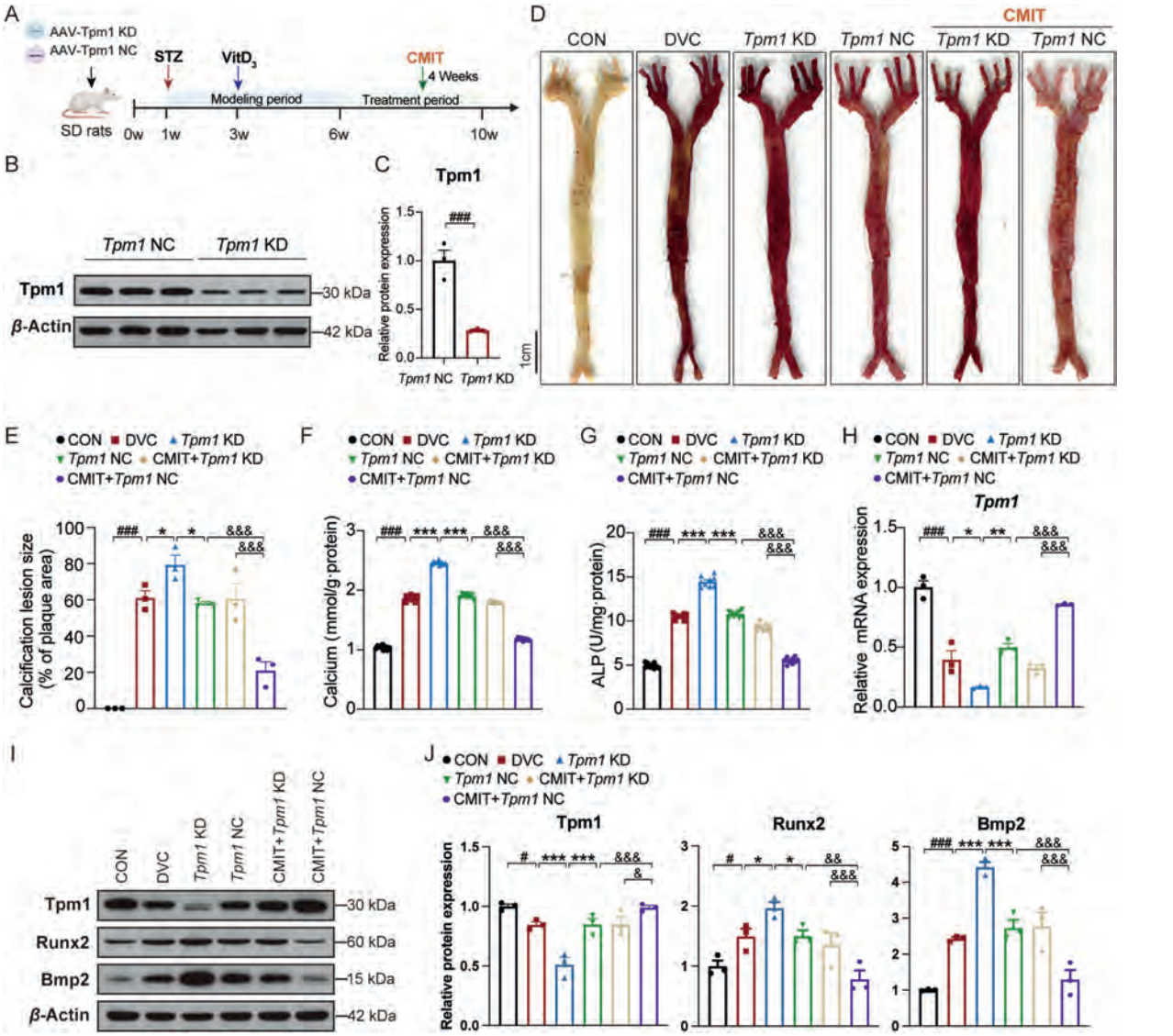

Figure 3 Knockdown of *Tpm1* aggravates arterial calcification *in vivo*. (A) Schematic diagram of animal experiments. Injecting AAV *Tpm1* KD/NC constructed *Tpm1* knockdown and control rat models *via* the tail vein. DVC was induced using STZ in combination with vitaminD_3 to observe the effect of *Tpm1* knockdown on the anti-calcification effect of CMIT; (B) Representative WB images of Tpm1 expression in the rat aorta of each group ($n = 3$); (C) Quantitative analysis of Tpm1 expression in (B) ($n = 3$); (D) Representative images of alizarin-red staining of the aorta of rats in each group ($n = 3$); (E) Quantitative alizarin-red staining of the entire aorta of rats in each group ($n = 3$); (F) Calcium content in the aorta of rats in each group (n = 9); (G) ALP activity in the aorta of rats in each group ($n = 9$); (H) *Tpm1* mRNA expression in the aorta of rats in each group ($n = 3$); (I) Representative WB images of Tpm1, Runx2 and BMP2 expressions in the aorta of rats in each group ($n = 3$); (J) Quantitative analysis of Tpm1, Runx2 and BMP2 expressions in (I) ($n = 3$). Data are expressed as mean ± SEM. Compared with the CON/*Tpm1* NC group, $^{\#}P < 0.05$, $^{\#\#\#}P < 0.001$; compared with the *Tpm1* KD group, $^{*}P < 0.05$, $^{**}P < 0.01$, $^{***}P < 0.001$; compared with the CMIT + *Tpm1* NC group, $^{\&}P < 0.05$, $^{\&\&}P < 0.01$, $^{\&\&\&}P < 0.001$.

calcification nodules in the aorta (Fig. 3D and E), increasing aortic calcium content and ALP levels (Fig. 3F and G), and upregulating the expression of osteogenic markers Runx2 and Bmp2, indicating that the lack of *Tpm1* worsens VC in diabetic rats (Fig. 3H−J). Notably, we found that the knockdown of *Tpm1* reversed the anti-DVC effects of CMIT (Fig. 3D−J). In conclusion, these results suggest that *Tpm1* is a key molecule in the development of DVC and a potential target for CMIT's action against DVC.

3.3. Tpm1 was negatively regulated by miR21-5p and was involved in the development of DVC

Gene expression regulation is a multilevel and complex process. We have identified the role of *Tpm1* in the development of DVC. Previous studies have shown that *Tpm1* plays a key role in a variety of vascular-related diseases as it is regulated by microRNAs (miRNAs)[27,28]. Since miRNAs are extensively involved in the regulation of multiple biological processes, including VC[29], bioinformatics approaches were adopted to further predict and validate the upstream miRNAs regulating *Tpm1*. *Tpm1*-targeted miRNAs were predicted by using DIANA-microT and miRTarBase, and the two databases produced a total of three intersecting miRNAs, including rno-miR21, rno-miR29, and rno-miR338 (Fig. 4A). Based on the research findings on these three miRNAs[8,30,31], the expressions of *miR21-5p*, *miR29c-3p*, and *miR338-3p* were further validated *in vivo* and *in vitro*. The results showed that *in vivo*, only *miR21-5p* was significantly upregulated in the aorta of rats with DVC (Fig. 4B). In the *in vitro* VSMCs model, *miR21-5p* expression progressively increased with the addition of high-glucose osteogenic medium. Notably, *miR21-5p* levels in the HGCM group were significantly higher than those in the HG group alone (Fig. 4C), suggesting that *miR21-5p* is markedly synergistic activated by high-glucose and calcification. Previously, *miR21-5p* was shown to directly target *Tpm1* and negatively regulate its expression in multiple disease models and cell lines[32-34]. Consistent with those reports, our results suggesting that *miR21-5p* may be a key upstream regulatory molecule through which *Tpm1* influences DVC. In addition, CMIT inhibits *miR21-5p* expression in rat aorta and in high-glucose calcified VSMCs (Fig. 4B, Fig. S5H and S5I).

To confirm the clinical association between the *miR21-5p*/*Tpm1* axis and DVC, *TPM1* and *miR21-5p* expressions were

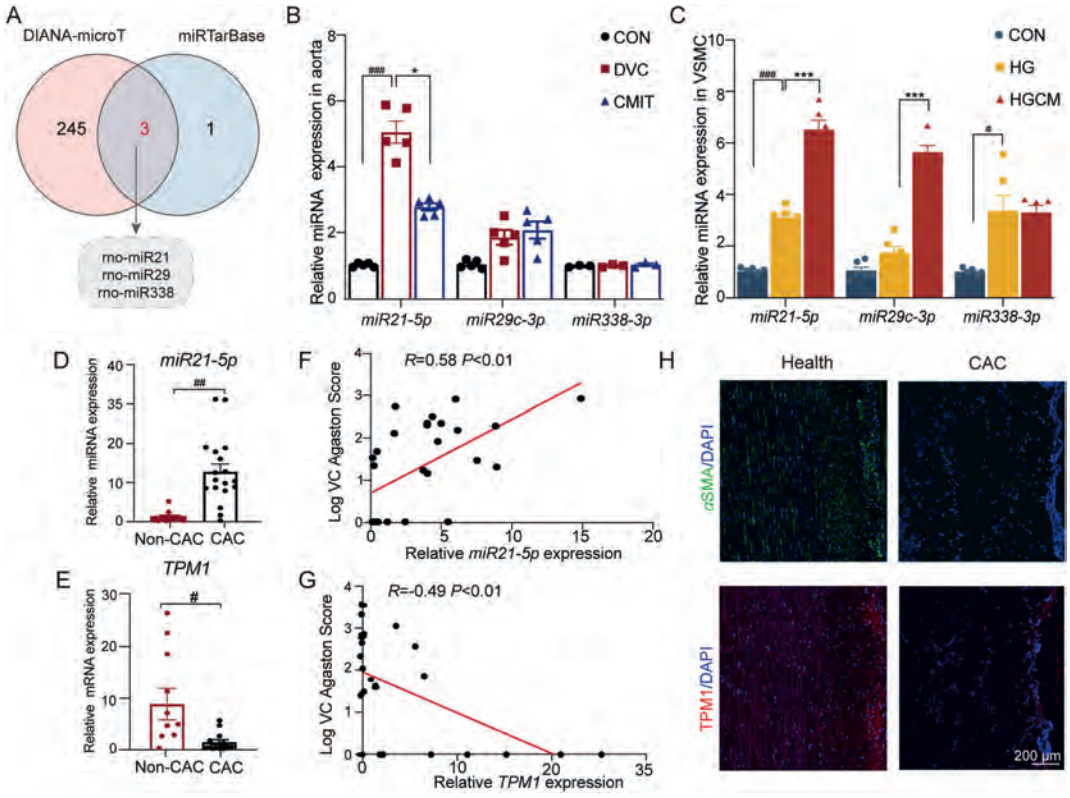

Figure 4 *TPM1* is negatively regulated by *miR21-5p* and is associated with an exacerbated risk of DVC. (A) Venn diagram showing the upstream miRNAs of *Tpm1* predicted using the DIANA-microT and miRTarBase databases; (B) Expression levels of *miR21-5p*, *miR29c-3p*, and *miR338-3p* in the rat aorta in each group (n = 3−5); (C) Expression levels of *miR21-5p*, *miR29c-3p*, and *miR338-3p* in the HAVSMC of each group (n = 6); (D) Expression of *miR21-5p* in the PBMCs of T2DM patients in the CAC and non-CAC groups (n (CAC) = 18, n (non-CAC) = 10); (E) Expression of *TPM1* in the PBMCs of T2DM patients in the CAC and non-CAC groups (n (CAC) = 18, n (Non-CAC) = 10); (F) Correlation between *miR21-5p* expression levels and VC scores in patients with T2DM (n = 28, with R-values and P-values of the Pearson correlation coefficient); (G) Correlation between *TPM1* expression levels and VC scores in patients with T2DM and CAC (n = 28, with R-values and P-values of the Pearson correlation coefficient). (H) Representative images of immunofluorescence staining of αSMA (green) and TPM1 (red) in the aortic sections from healthy volunteers and patients with T2DM with CAC, and the cell nuclei were re-stained with DAPI (blue) (n = 3, 10 ×). DAPI: diamidino phenylindole, CAC: coronary artery calcification. Data are expressed as mean ± SEM. Compared with the CON or NG or Non-CAC groups, $^{\#}P < 0.05$, $^{\#\#}P < 0.01$, $^{\#\#\#}P < 0.001$. Compared with DVC or HG groups, $^{*}P < 0.05$, $^{***}P < 0.001$.

examined using mRNA from PBMCs of 28 patients with diabetes with or without CAC (Fig. 4D−G). The CAC scores were significantly higher in T2DM patients with CAC compared to those without CAC (424.00 (57.50, 856.75) *vs.* 0.00 (0.00, 0.00)). Compared with patients with diabetes without VC, there were more male patients with diabetes with VC, and the *miR21-5p* levels in the peripheral blood were significantly increased (Fig. 4D, Supporting Information Table S5, 1.00 ± 0.53 *vs.* 4.64 ± 0.86, $P < 0.01$). In contrast, *TPM1* levels were significantly decreased (Fig. 4E, Table S5, 8.61 ± 3.03 *vs.* 1.31 ± 0.49, $P < 0.01$). Moreover, *miR21-5p* expression was positively correlated with the coronary VC Agatston score in patients with DVC (Fig. 4F, $P < 0.01$). In contrast, *TPM1* expression was negatively correlated with the coronary VC Agatston score (Fig. 4G, $P < 0.01$). There were no significant differences in other traditional cardiovascular risk factors (blood pressure, heart rate, smoking and alcohol consumption, and lipid metabolism), serum calcium and phosphorus levels, and renal function between the two groups ($P > 0.05$). In addition, immunofluorescence staining was performed for TPM1 and αSMA in the aortas of patients with diabetic CAC and healthy volunteers for validation. As expected, the expressions of TPM1 and the contractile marker αSMA were consistently decreased in calcified arteries (Fig. 4H). In conclusion, these data collectively suggested that the *miR21-5p/Tpm1* axis is involved in the progression of DVC and may be a key pathway for the anti-DVC effect of CMIT.

3.4. Overexpression of miR21-5p promoted osteogenic differentiation of VSMC through Tpm1 downregulation

VSMCs are the main site for the onset of DVC, and the differentiation from a contractile to an osteogenic phenotype is a critical part of VC onset. Next, we examined whether *miR21-5p/Tpm1* affected the osteogenic differentiation of VSMCs. The effects of *miR21-5p* on cell function and calcification of VSMCs were observed by transfecting the *miR21-5p* mimic, the *miR21-5p* inhibitor, and the corresponding NC (Fig. 5A). The results showed that the *miR21-5p* mimic significantly upregulated *miR21-5p* expression in VSMCs, while the *miR21-5p* inhibitor significantly inhibited *miR21-5p* expression in VSMCs, indicating that the transfection was successful (Fig. 5B). CCK-8 and scratch assays showed that compared with the NG group, VSMC proliferation and migration were significantly enhanced in the HGCM group (Fig. 5C and D). Compared with cells in the HGCM group, overexpression of *miR21-5p* further enhanced the proliferation and migration of VSMCs, while inhibition of *miR21-5p* ameliorated the excessive proliferation and migration of VSMCs (Fig. 5C and D).

Alizarin red staining showed that the cells in the HGCM group demonstrated scattered dark red calcified nodules compared with the NG group after 7 days of induction with high glucose osteogenic medium. Compared with the HGCM group, calcification was enhanced in cells in the *miR21-5p* mimic group, while no significant calcified nodules were observed in the *miR21-5p* inhibitor group (Fig. 5E). In addition, the calcium content of HAVSMCs in each group was determined by colorimetric assay, and the calcium content of cells in the HGCM group was significantly higher than that in the NG group. Compared with cells in the HGCM group, the calcium content of cells in the *miR21-5p* mimic group was further increased. In contrast, that of cells in the *miR21-5p* inhibitor group was significantly decreased, which was consistent with the results of alizarin red staining (Fig. 5F). These findings indicated that overexpression of *miR21-5p* promoted VSMC calcification *in vitro*, while inhibition of *miR21-5p* inhibited this process. Next, the levels of contractile and osteogenic proteins in HAVSMCs in each group were further examined. As expected, *miR21-5p* overexpression promoted the osteogenic differentiation of VSMCs, including upregulation of osteogenic proteins RUNX2 and BMP2, as well as downregulation of contractile proteins αSMA and SM22α (Fig. 5G and H). Inhibition of *miR21-5p* reversed this process (Fig. 5G and H). It was further found that *miR21-5p* downregulated *TPM1* expression in VSMCs at both transcriptional and protein levels (Fig. 5I−L), which was consistent with the results of a previous study[35]. These findings suggested that *miR21-5p* was a key regulator of the osteogenic differentiation of VSMCs, and the regulation was possibly achieved through regulating the downstream target *TPM1*.

3.5. Tpm1 silencing eliminated the anti-osteogenic differentiation effect of miR21-5p inhibitor for VSMCs

To verify whether the regulation of VSMC osteogenic differentiation by *miR21-5p* requires mediation by *TPM1*, the effects of *TPM1* siRNA on the function and osteogenic differentiation of VSMC were examined with silenced *miR21-5p*. Compared with cells transfected with control siRNA, *TPM1* expression was significantly downregulated in VSMCs transfected with *TPM1* siRNA (Fig. 6A). CCK-8 and scratch assays showed that *TPM1* siRNA significantly eliminated the inhibitory effect of the *miR21-5p* inhibitor for the hyperproliferation and migration of cells (Fig. 6B−D). Similarly, alizarin red staining and calcium content assay showed that *TPM1* siRNA blocked the inhibitory effect of the *miR21-5p* inhibitor on VSMC calcification (Fig. 6E and F). In addition, WB results showed that the downregulation of BMP2 and RUNX2 expressions, as well as the upregulation of αSMA and SM22α expressions in VSMCs by the *miR21-5p* inhibitor, were also inhibited by *TPM1* siRNA (Fig. 6G and H). PCR and WB assays further confirmed the direct negative regulatory relationship between *miR21-5p* and *TPM1* (Fig. 6I−L). In conclusion, these findings suggest that *Tpm1* plays a key role in the regulation of osteogenic differentiation of VSMC by *miR21-5p*. Inhibition of the *miR21-5p/Tpm1* axis may be a potential strategy for treating osteogenic differentiation of VSMC and DVC.

3.6. Overexpression of miR21-5p reversed the anti-DVC effect of CMIT

To further determine the role of the *miR21-5p/Tpm1* axis in the CMIT treatment of DVC, an AAV-*miR21-5p* overexpression driven by U6 promoter was constructed to induce the overexpression of *miR21-5p* in rats (Fig. 7A). AAV-*miR21-5p* overexpression/NC was injected intravenously *via* the tail vein 1 week after STZ injection, and CMIT therapy was performed for 4 weeks continuously starting from 4 weeks after the injection (Fig. 7A). The injection of AAV-*miR21-5p* OE can significantly increase the expression of *miR21-5p* in rat aorta (Fig. 7B). During the experiment, compared with the CON group, a substantial increase in blood glucose level and a significant decrease in body weight were observed in the DVC group (Supporting Information Fig. S6A−S6D), and the fluctuations of body weight and blood glucose level in the intervention groups were comparable to those in the DVC group. Whereas in terms of food intake, no significant effects of calcification and fasting were observed (Fig. S6E and S6F). Alizarin red staining showed that overexpression of

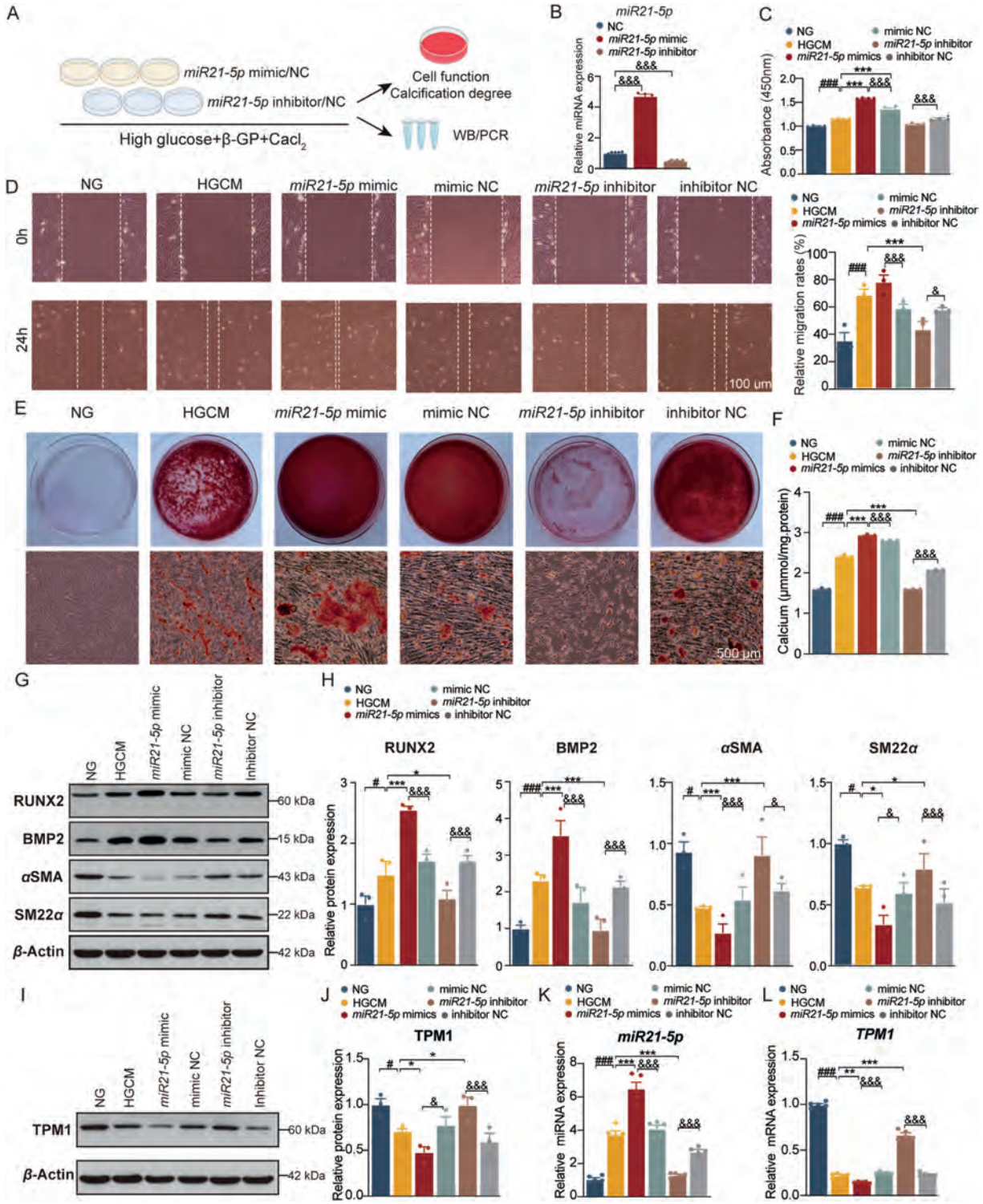

Figure 5 *miR21-5p* promotes osteogenic differentiation of VSMCs by regulating *Tpm1*. (A) Schematic diagram of the cellular experiments. *In vitro*, calcification of HAVSMCs was induced by using high glucose and osteogenic medium. The calcified HAVSMCs were treated with *miR21-5p* mimic or inhibitor, respectively, and the corresponding NC groups were set to observe the cell function, degree of calcification, and expression level of contractile proteins; (B) Expression level of *miR21-5p* after transfection with *miR21-5p* mimic or inhibitor ($n = 6$); (C) CCK-8 assay to determine the proliferative activity of HAVSMCs in each group ($n = 3$); (D) Left: scratch assay to determine cell migration of HAVSMCs in each group at 24 h ($n = 3$, 20 ×), right: migration rate of HAVSMCs in each group ($n = 3$); (E) Representative images of alizarin red staining of HAVSMCs in each group ($n = 3$). The upper panel shows the overall calcification staining in the culture dishes of different treatment groups, and the lower panel shows the calcified areas observed under the microscope (4 ×); (F) Calcium content of HAVSMCs in each group ($n = 3$); (G) Representative WB images of RUNX2, BMP2, αSMA, and SM22α expressions in the HAVSMCs in each group ($n = 3$); (H)

miR21-5p significantly aggravated VC in diabetic rats. Although CMIT therapy alleviated VC to a large extent, the above protective effect was eliminated when *miR21-5p* was overexpressed (Fig. 7C−F). Then, the serum calcium, phosphorus, and ALP levels of rats in each group were examined. Compared with the CON group, the serum calcium, phosphorus, and ALP levels of rats in the DVC group were significantly increased. *miR21-5p* overexpression further increased the serum calcium levels of rats but had little effect on serum phosphorus and ALP levels. Meanwhile, no significant impact of CMIT therapy on serum calcium, phosphorus, and ALP levels was observed (Fig. 7G−I). In addition, aortic calcium levels and ALP activity in rats with *miR21-5p* overexpression were significantly higher than those in rats of the DVC group and the corresponding NC groups. CMIT therapy was effective in decreasing aortic calcium levels, and ALP activity; however, the above effects were suppressed after *miR21-5p* overexpression (Fig. 7J and K). Similarly, *miR21-5p* overexpression also significantly promoted the osteogenic differentiation of VSMC *in vivo*. CMIT therapy inhibited the osteogenic differentiation of VSMC in rat aorta, including the downregulation of Bmp2 and Runx2 expressions as well as the upregulation of αSMA and Sm22α expressions. However, the above effects disappeared after *miR21-5p* overexpression (Fig. 7L and M). These findings suggested that the *miR21-5p/Tpm1* axis is essential for the treatment of DVC by CMIT.

3.7. CMIT inhibited the activation of the miR21-5p/Tpm1 axis in vivo

Next, the effects of the CMIT therapy on the aortic *miR21-5p/Tpm1* axis at the transcriptional and protein levels were observed. As expected, the CMIT therapy significantly decreased aortic *miR21-5p* levels (Fig. 8A), restored *miR21-5p*-mediated downregulation of *Tpm1* and the contractile phenotype of VSMCs (Fig. 8B−F), and inhibited the activation of the *miR21-5p/Tpm1* axis *in vivo* (Fig. 8A−C and G). All these findings suggested that CMIT exerted a therapeutic effect on DVC by inhibiting the activation of the *miR21-5p/Tpm1* axis and preventing the osteogenic transformation of VSMC.

4. Discussion

VC is a vascular pathological marker and predictor of cardiovascular risk in patients with diabetes[36]. Early prevention and treatment of VC are important for preventing advanced target organ damage. However, due to its variable clinical manifestations and complex pathogenesis, there has still been a lack of effective therapeutic options. Previous studies have shown that early intervention with TCM can effectively slow the progression of VC, preserve vascular integrity, and serve as an important strategy for preventing damage to target organs such as the heart and kidney[37]. However, since VC results from the accumulation of multiple metabolic risk factors, pharmacological treatment alone is often insufficient to achieve long-term disease control. Therefore, incorporating healthy lifestyle management is essential to complement the clinical prevention and treatment of VC. IF as an effective dietary intervention, is increasingly recognized as a promising approach to alleviating various cardiometabolic disorders[38], particularly in individuals with metabolic conditions such as diabetes. Moreover, IF has the potential to reduce the dosage requirements of medications in diabetic patients, thereby showing great promise as part of a combination therapy[39]. However, the metabolic benefits of IF are closely tied to caloric intake and are significantly influenced by patient adherence over time. Individuals may develop compensatory behaviors such as “rebound eating”, which could diminish or even negate the beneficial metabolic effects of IF[40]. Emerging evidence indicates that although IF can initially reduce blood glucose levels in severe diabetic mouse models, after approximately four months of sustained intervention, these mice develop “IF-resistant” characterized by rising blood glucose levels and reduced autophagic flux[41]. These findings suggest that relying solely on IF may be insufficient for the stable and sustained management of chronic metabolic diseases, underscoring the need for more robust and synergistic combination strategies.

In this study, we innovatively proposed a combined intervention integrating TCM and IF, and established a comprehensive therapeutic approach—CMIT—for the prevention and management of DVC. This approach aims to alleviate the medication burden in diabetic patients through IF, while leveraging the multitarget regulatory effects of TCM to reinforce and prolong the metabolic benefits conferred by IF. Among them, TCM with DLTM has been proven to be effective in improving VC in diabetic rats during the early stage[3]. At the same time, IF has been shown to exert significant therapeutic effects on systemic and micro-vascular dysfunction in DM[8]. The efficacy of CMIT in improving calcium and phosphorus metabolism and ameliorating VC in diabetic rats was significantly better than that of DLTM and IF monotherapies. In terms of mechanism of action, the effects of CMIT were related to the regulation of the *miR21-5p/Tpm1* axis, as CMIT prevented the osteogenic differentiation of VSMC by inhibiting the activation of the *miR21-5p/Tpm1* axis, thus improving DVC.

Diabetes-induced systemic metabolic disorders, including imbalances in blood glucose and calcium and phosphorus metabolism, are the initiating factors of VC[36]. Hyperglycemia induces local oxidative stress and endothelial cell dysfunction through abnormal glucose metabolism pathway[42], which stimulates excessive migration, proliferation, and osteogenic differentiation of VSMCs in the tunica media[43]. The imbalance of calcium and phosphorus metabolism is also a key factor for pathological VC onset[44-46]. In this study, significant disorders of the blood glucose and calcium-phosphorus metabolism, as well as elevated FBG, serum calcium, and ALP levels, were observed in rats with DVC, which corresponded to severe VC injury. DLTM, IF, and CMIT interventions partially ameliorated VC and reduced serum calcium and ALP levels in diabetic rats. In particular, CMIT was superior to DLTM and IF monotherapies in improving calcium-phosphorus metabolism and reducing VC area, suggesting that DLTM and IF

Quantitative analysis of RUNX2, BMP2, αSMA, and SM22α expressions in (G) ($n = 3$); (I) Representative WB images of TPM1 expression in HAVSMCs in each group ($n = 3$); (J) Quantitative analysis of TPM1 expression in I ($n = 3$); (K) *miR21-5p* expression levels in HAVSMCs in each group ($n = 3$); (L) *TPM1* mRNA levels in HAVSMCs in each group ($n = 3$). Data are expressed as mean ± SEM. Compared with NG, $^{\#}P < 0.05$, $^{\#\#\#}P < 0.001$. Compared with the HGCM group, $^{*}P < 0.05$, $^{**}P < 0.01$, $^{***}P < 0.001$. Compared with mimic/inhibitor in the NC group. $^{\&}P < 0.05$, $^{\&\&\&}P < 0.001$.

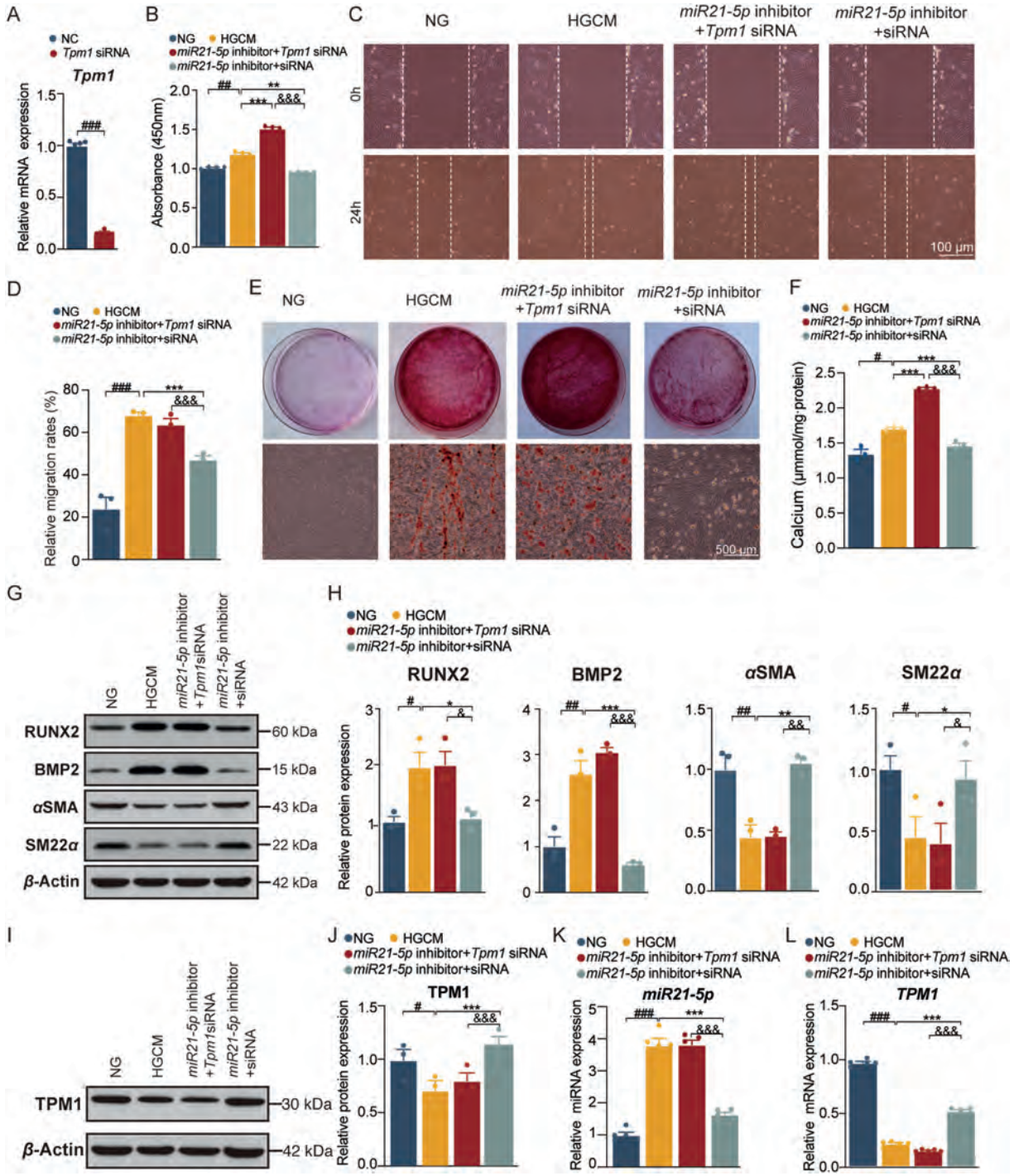

Figure 6 *TPM1* silencing counteracts the effect of *miR21-5p* inhibitor on the osteogenic differentiation of VSMC. (A) The mRNA expression level of *TPM1* after transfection with *TPM1* siRNA or siRNA ($n = 6$); (B) CCK-8 assay to determine the proliferative activity of HAVSMCs in each group ($n = 3$); (C) A scratch assay to determine the cell migration of HAVSMCs in each group at 24 h ($n = 3$, 20 ×); (D) HAVSMCs migration rates in each group ($n = 3$); (E) Representative images of alizarin red staining of HAVSMCs in each group ($n = 3$). The upper graph shows the overall calcification staining in culture dishes of different treatment groups, while the lower graph shows the calcified area observed under the microscope (4 ×); (F) Calcium content of HAVSMCs in each group ($n = 3$); (G) Representative WB images of RUNX2, BMP2, αSMA, and SM22α expressions in the HAVSMCs in each group ($n = 3$); (H) Quantitative analysis of RUNX2, BMP2, αSMA, and SM22α expressions in G ($n = 3$); (I) Representative WB images of TPM1 expression in HAVSMCs in each group ($n = 3$); (J) Quantitative analysis of TPM1 expression in (I) ($n = 3$); (K) *miR21-5p* expression level in each group of HAVSMCs ($n = 3$); (L) *TPM1* mRNA levels in HAVSMCs in each group ($n = 3$). Data are expressed as mean ± SEM. Compared with NG, $^{\#}P < 0.05$, $^{\#\#}P < 0.01$, $^{\#\#\#}P < 0.001$; compared with the HGCM group, $^{*}P < 0.05$, $^{**}P < 0.01$, $^{***}P < 0.001$; compared with *miR21-5p* inhibitor + siRNA, $^{\&}P < 0.05$, $^{\&\&}P < 0.01$, $^{\&\&\&}P < 0.001$.

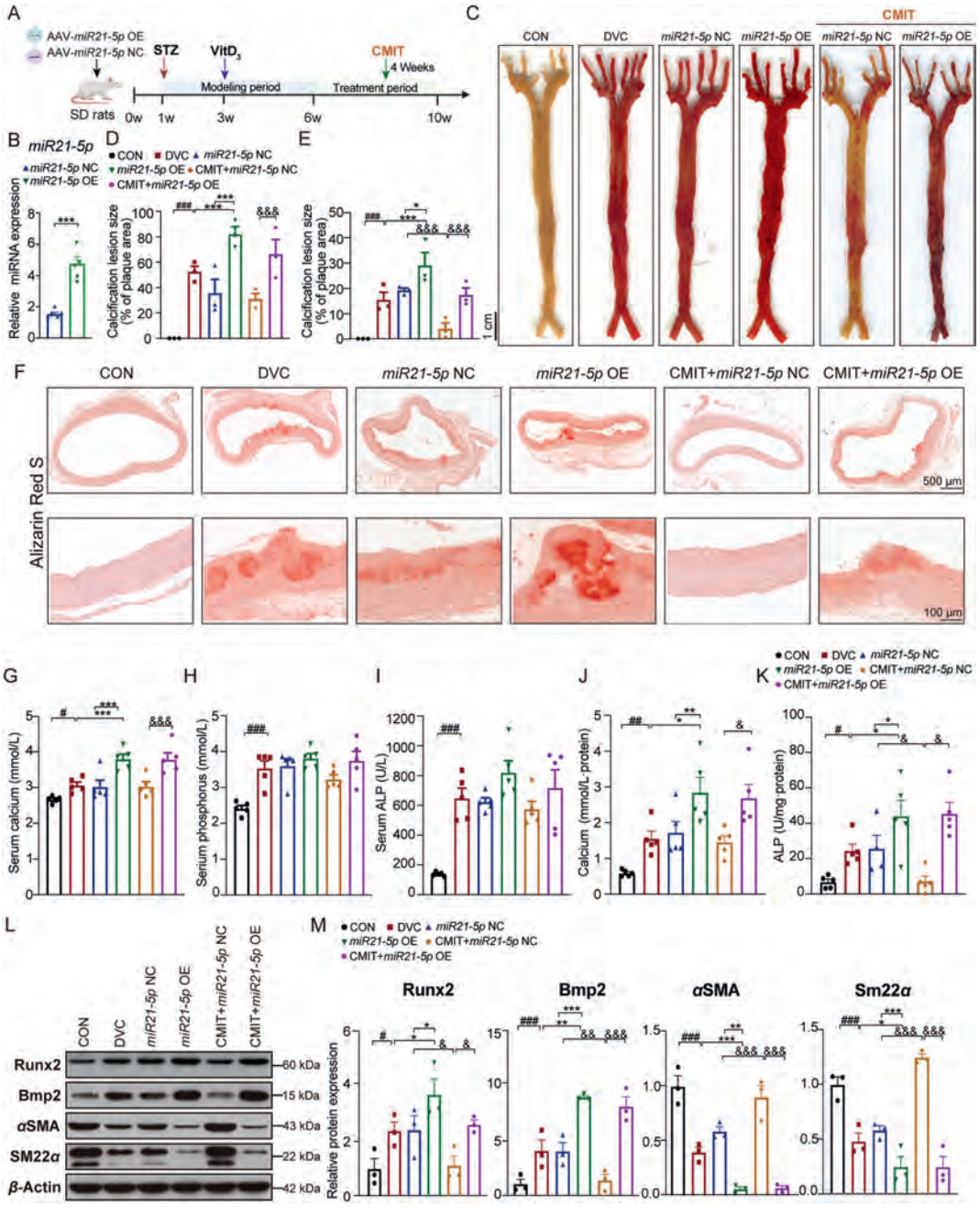

Figure 7 *MiR21-5p* overexpression eliminates the anti-VC effect of CMIT. (A) Schematic diagram of animal experiments. Injecting AAV *miR21-5p* overexpression/NC constructed *miR21-5p* overexpression and control rat models *via* the tail vein. DVC was induced using STZ in combination with vitamin D3 to observe the effect of *miR21-5p* overexpression on the anti-calcification effect of CMIT; (B) Expression levels of *miR21-5p* in the rat aorta in *miR21-5p* NC and *miR21-5p* OE group ($n = 5$); (C) Representative image of the alizarin red pathological staining of the entire aorta in each group of rats ($n = 3$); (D) Quantification of alizarin red staining of the entire aorta ($n = 3$); (E) Quantification of alizarin red staining of the aortic arch of rats in each group ($n = 3$); (F) Representative images of alizarin red staining of the aortic arch of rats in each group ($n = 3$); (G) Serum calcium level of rats in each group ($n = 5$); (H) Serum phosphorus level of rats in each group ($n = 5$); (I) Serum ALP level of rats in each group ($n = 5$); (J) Aortic calcium level of rats in each group ($n = 5$); (K) Aortic ALP activity of rats in each group ($n = 4-5$); (L) Representative WB images of Runx2, Bmp2, αSMA, and Sm22α expressions in the aorta of rats in each group ($n = 3$); (M) Quantitative analysis of Runx2, Bmp2, αSMA, and Sm22α expressions in (L) ($n = 3$). Data are expressed as mean ± SEM. Compared with CON $^{\#}P < 0.05$, $^{\#\#}P < 0.01$, $^{\#\#\#}P < 0.001$; compared with the DVC group, $^{*}P < 0.05$, $^{**}P < 0.01$, $^{***}P < 0.001$. Compared with the CMIT + *miR21-5p* NC group, $^{\&}P < 0.05$, $^{\&\&\&}P < 0.01$, $^{\&\&\&}P < 0.001$.

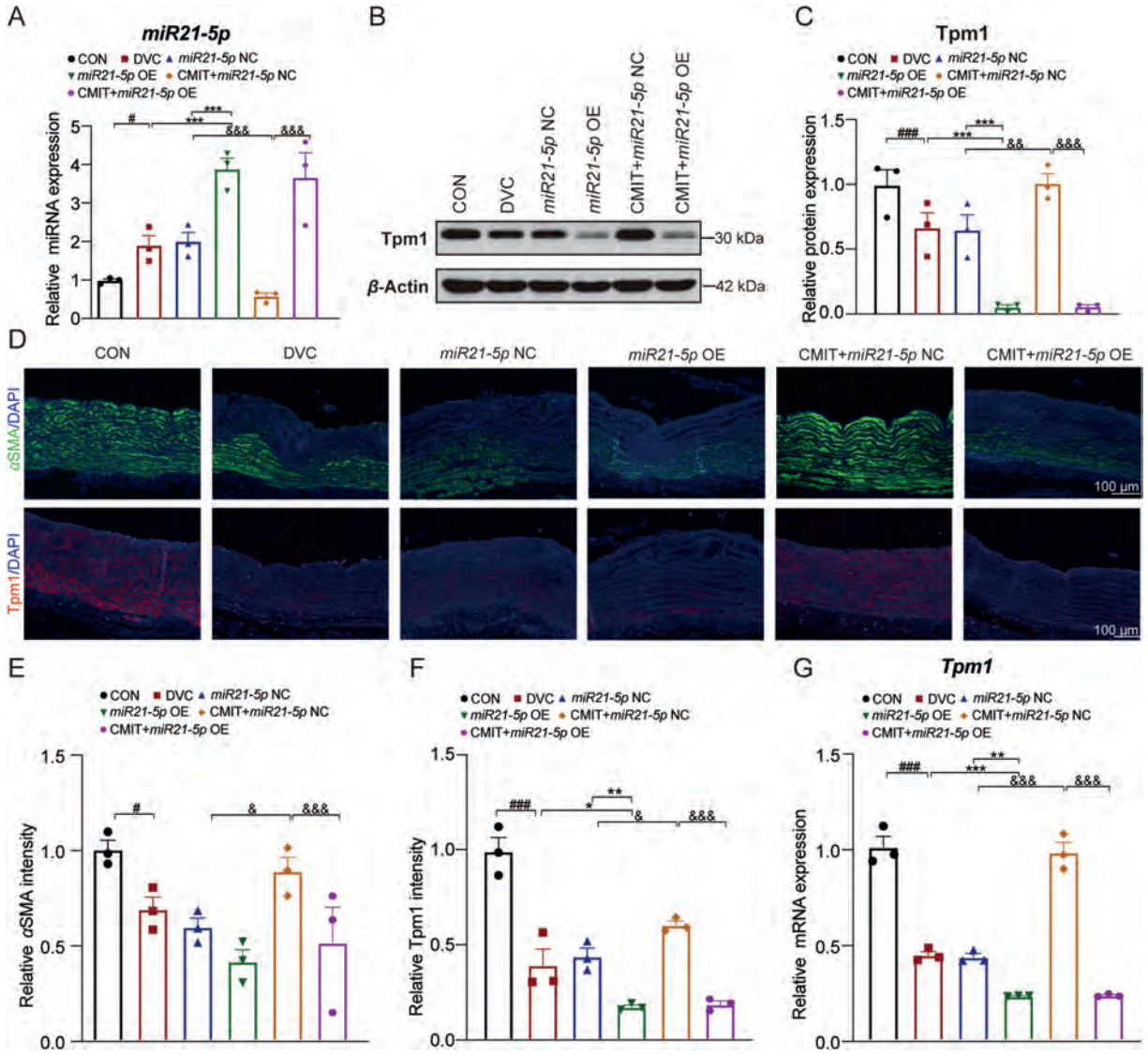

Figure 8 *MiR21-5p/Tpm1* axis mediates the anti-DVC effect of CMIT. (A) Expression levels of *miR21-5p* in the rat aorta in each group ($n = 3$); (B) Representative WB images of Tpm1 expression in the rat aorta in each group ($n = 3$); (C): Quantification of Tpm1expression in the rat aorta in each group in (B) ($n = 3$); (D) Representative images of immunofluorescent staining of αSMA (green) and Tpm1 (red) in rat aortic sections in each group, with cell nuclei re-stained with DAPI (blue) ($n = 3$, 20 ×); (E) Quantitative analysis of fluorescence intensity of *αSMA* in (D) ($n = 3$); (F) Quantitative analysis of fluorescence intensity of Tpm1 in (D) ($n = 3$); (G) *Tpm1* mRNA levels in the rat aorta in each group ($n = 3$). DAPI: diamidino phenylindole. Data are expressed as mean ± SEM. Compared with CON, $^{\#}P < 0.05$, $^{\#\#\#}P < 0.001$; compared with the DVC group, $^{**}P < 0.01$, $^{***}P < 0.001$; compared with the CMIT + *miR21-5p* NC group, $^{\&}P < 0.05$, $^{\&\&}P < 0.01$, $^{\&\&\&}P < 0.001$.

synergistically enhanced the regulation of calcium-phosphorus homeostasis and vascular repair. In addition, we independently identified the anti-calcification prototype compounds in DLTM and simulated the effect of CMIT on VSMCs *in vitro* by combining these compounds with intermittent serum deprivation. Consistent with the *in vivo* findings, co-treatment with IF significantly enhanced the effects of DLTM compounds (resveratrol, rosmarinic acid, tanshinone IIA, etc.) in inhibiting excessive cell proliferation and reducing intracellular calcium levels. These results further support the potential of CMIT to inhibit calcium deposition and delay the progression of vascular calcification both *in vivo* and *in vitro*. These findings prompted a deeper investigation into the molecular targets and mechanisms underlying CMIT's therapeutic effects.

Transcriptomics sequencing is important for understanding TCM combinations with multiple targets as well as therapeutic regimens combining multiple interventions, as it can comprehensively reveal the dynamics of the gene regulatory network of the organism[47]. In this study, CMIT significantly affects the aortic transcriptome profile of rats with DVC, involving more DEGs than that of DLTM and IF. Enrichment analysis showed that these DEGs affected a large number of biological processes and pathways, including cardiac contractile regulation and muscle cell development, which were also related to the phenotypic transformation of VSMCs[48], calcium signaling malfunctions[49], and

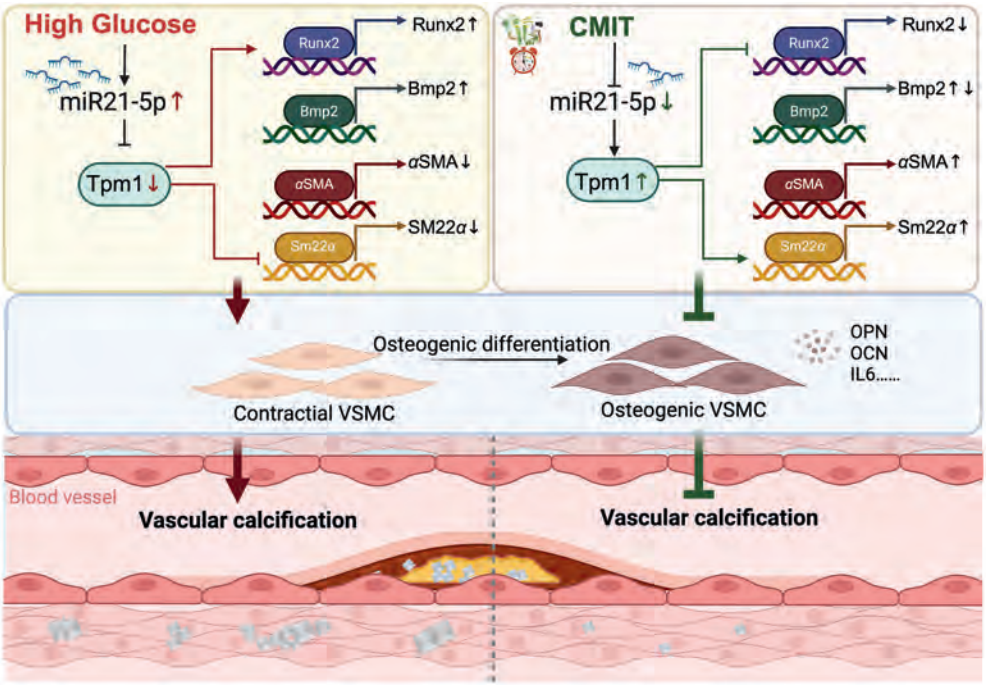

Figure 9 CMIT alleviates vascular calcification by inhibiting the activation of *miR21-5p*/*Tpm1* axis.

hemodynamic disorders[50] during the onset of VC. Through PPI analysis, attention was drawn to *Tpm1*. *Tpm1* belongs to the tropomyosin family. It is an actin-binding protein that is widely distributed in cells and regulates cell shape, strength, and molecular signaling by modulating the interaction between actin and myosin[26]. Recently, *Tpm1* has been found to be closely related to the state and phenotypic transformation of VSMC. The gene expression of *Tpm1* in rabbit VSMC was correlated with the dedifferentiated state of VSMC, and the upregulation of *Tpm1* suggested the transformation of VSMC into a contractile phenotype[51]. Activation of endogenous *Tpm1* inhibited tissue necrosis factor-α-induced inflammatory response in VSMC, reduced the expression of adhesion molecules vascular cell adhesion molecule-1 and intercellular adhesion molecule-1, and downregulated the levels of intranuclear inflammatory genes NFκB and CCN4, thus maintaining the normal contractile phenotype of VSMC[52]. In this study, significant downregulation of *Tpm1* was observed in the aorta of rats with DVC, in an *in vitro* model of VSMC calcification, as well as in the peripheral blood and aorta of patients with diabetic CAC. The impact of such a phenomenon was closely related to the osteogenic differentiation of VSMC. CMIT also has an independent regulatory effect on *Tpm1* as it could reverse the downregulation of *Tpm1* induced by DVC. Subsequently, we further confirmed that *in vivo* knockdown of *Tpm1* exacerbated arterial calcification and simultaneously abolished the anti-calcification effects of CMIT. These findings provide direct evidence that *Tpm1* serves as a critical target mediating the therapeutic efficacy of CMIT against vascular calcification.

The regulation of gene expression is usually affected by multiple mechanisms. As important upstream regulators, miRNAs can bind to the 3′UTR of mRNAs and regulate gene expression by destabilizing mRNAs or affecting the translation efficiency of mRNAs[53]. Previous studies have shown that miRNAs regulate *Tpm1* to influence the progression vascular diseases such as atherosclerosis and vascular dementia[54,55]. Therefore, bioinformatics analysis was performed to further explore whether miRNAs are involved in regulating *Tpm1* expression in DVC. It was found that *miR21-5p* negatively regulated *Tpm1* to promote calcification *in vivo* and *in vitro*. *miR21-5p* was closely involved in the osteogenic differentiation of cells. It promoted osteogenic differentiation by improving the development of the actin cytoskeleton, promoting the expression of osteogenic markers, and inhibiting osteoblast maturation[56,57]. Previous dual-luciferase assays demonstrated that the seed sequence of *Tpm1* in the mRNA 3′-UTR is complementary to *miR21-5p*[58], providing direct evidence that *Tpm1* is a downstream target mRNA of *miR21-5p*. Furthermore, studies have shown that the activation of *miR21-5p* in the aorta reduces cytoskeletal stability and promotes the phenotypic transformation, migration, and proliferation of VSMC through the downregulation of *Tpm1*[35]. other research indicates that *miR21-5p* targeting *Tpm1* is involved in high glucose-induced VSMC osteogenic differentiation. Under high glucose conditions, *miR21-5p* is activated, inhibiting the expression of its downstream target *Tpm1*. This activation leads to downregulation of the contractile protein αSMA and upregulation of the osteogenic protein OPN, promoting the transformation of VSMCs into an osteogenic phenotype[59]. This study also showed that *miR21-5p* overexpression significantly reduced the mRNA and protein levels of *Tpm1*, which led to the over-proliferation, migration, and calcification of VSMCs, which in turn aggravated DVC. Tpm1 is an actin-binding protein and is closely related to the formation, stabilization, and regulation of cytoskeletal actin filaments. Cytoskeletal reorganization, a process mediated by *Tpm1*, is essential for cell shape change, cell proliferation, and migration[60,61]. *Tpm1* deficiency would result in the dysregulation of the movement and contraction of actin filaments, which may lead to cytoskeletal reorganization, resulting in cell proliferation and excessive migration[62]. Meanwhile, the downregulation of *Tpm1* also inhibits the stable binding of αSMA in stress fibers, resulting in reduced contractile properties and enhanced phenotypic differentiation

potential of myocytes[63]. We hypothesized that overexpression of *miR21-5p* would lead to significant inhibition of *Tpm1* and further downregulation of the contractile proteins αSMA and Sm22α, leading to the destabilization of cellular stress fibers. Such structural change was accompanied by a significant upregulation of the expressions of osteogenic proteins Runx2 and Bmp2, which promoted the differentiation of VSMC toward an osteogenic phenotype and ultimately led to the production of calcification nodules and the massive deposition of calcium salts, resulting in VC.

Furthermore, to elucidate whether the anti-calcification effect of CMIT is associated with the *miR21-5p*/*Tpm1* axis-mediated phenotypic transformation of VSMCs, we established rat models with either *miR21-5p* overexpression or negative control using AAV, followed by CMIT intervention. Our findings reveal that, compared to the control group, rats with *miR21-5p* overexpression exhibited a significant exacerbation of DVC and a concurrent downregulation of *Tpm1* expression in the aorta. Importantly, CMIT therapy inhibits the activation of *miR21-5p* in the aorta and restores the expression level of *Tpm1*. This restoration inhibited VSMC osteogenic differentiation, thereby alleviating DVC. Notably, in the context of *miR21-5p* overexpression, the anti-DVC effects of CMIT were completely reversed. These results suggest that CMIT exerted its anti-DVC effects by inhibiting *miR21-5p*/*Tpm1* axis-mediated osteogenic differentiation of VSMCs (Fig. 9).

A limitation of this study was that only the effect of time-restricted fasting in combination with DLTM was tested, and the effect of alternate-day fasting or other IF methods in combination with DLTM on ameliorating DVC was not explored. Additionally, the upstream transcriptional regulators of *miR21-5p* expression, which modulate its effects on cytoskeletal targets, remain unidentified. Besides *Tpm1*, *miR21-5p* also acts on other cytoskeletal proteins, such as Gelsolin[64]. Studies have shown a direct association between gelsolin and the progression of abdominal aortic calcification[65]. The synergistic role of *Tpm1*, gelsolin, and other cytoskeletal proteins in the regulation of VC should be investigated in the future.

5. Conclusions

In this study, we proposed and demonstrated for the first time that combining TCM and IF prevents the osteogenic differentiation of VSMC by inhibiting the activation of the *miR21-5p*/*Tpm1* axis, thus exerting therapeutic effects on DVC, which provided new evidence for combining TCM and diet in the prevention and treatment of patients with DVC.

Acknowledgments

This work was supported by National Science Foundation of China (82405156), Excellent Young Science and Technology Talent Cultivation Special Project of CACMS (CI2023D006, China), and Hospital capability enhancement project of Xiyuan Hospital of CACMS (Nos. XYZX0201-10 and XYZX0405-21, China).

Author contributions

Yue Liu contributed to the conceptualization, manuscript revision, and the decision to submit for publication. Wenting Wang, Yanfei Liu, Yiwen Li performed the experiments and analysed the data, Qian Xu, Mengmeng Zhu and Jing Cui analysed the data, Wenting Wang drafted the manuscript, Yanfei Liu help to revise the manuscript. All authors approved the final version of the manuscript.

Conflicts of interest

The authors declare no conflicts of interest.

Appendix A. Supporting information

Supporting information to this article can be found online at https://doi.org/10.1016/j.apsb.2025.11.016.

References

1. Ghosh S, Luo D, He W, Chen J, Su X, Huang H. Diabetes and calcification: the potential role of anti-diabetic drugs on vascular calcification regression. *Pharmacol Res* 2020;**158**:104861.
2. Zhang Y, Wu J, Liu Y, Liu Y. Cardiovascular 1.5-level prevention: a comprehensive screening and intervention for early cardiovascular organ damage. *Sci Bull* 2025;**70**:1380−3.
3. Wang W, Li Y, Zhu M, Xu Q, Cui J, Liu Y, et al. Danlian-Tongmai formula improves diabetic vascular calcification by regulating CCN3/NOTCH signal axis to inhibit inflammatory reaction. *Front Pharmacol* 2025;**15**:1510030.
4. Wang W, Liu Y, Li Y, Luo B, Lin Z, Chen K, et al. Dietary patterns and cardiometabolic health: clinical evidence and mechanism. *MedComm* 2023;**4**:e212.
5. Che T, Yan C, Tian D, Zhang X, Liu X, Wu Z. Time-restricted feeding improves blood glucose and insulin sensitivity in overweight patients with type 2 diabetes: a randomised controlled trial. *Nutr Metab* 2021;**18**:88.
6. Guo Y, Luo S, Ye Y, Yin S, Fan J, Xia M. Intermittent fasting improves cardiometabolic risk factors and alters gut microbiota in metabolic syndrome patients. *J Clin Endocrinol Metab* 2021;**106**:64−79.
7. Cui J, Lee S, Sun Y, Zhang C, Hill MA, Li Y, et al. Alternate day fasting improves endothelial function in type 2 diabetic mice: role of adipose-derived hormones. *Front Cardiovasc Med* 2022;**9**:925080.
8. Hammer SS, Vieira CP, McFarland D, Sandler M, Levitsky Y, Dorweiler TF, et al. Fasting and fasting-mimicking treatment activate SIRT1/LXRα and alleviate diabetes-induced systemic and microvascular dysfunction. *Diabetologia* 2021;**64**:1674−89.
9. Yang X, Zhou J, Shao H, Huang B, Kang X, Wu R, et al. Effect of an intermittent calorie-restricted diet on type 2 diabetes remission: a randomized controlled trial. *J Clin Endocrinol Metab* 2023;**108**:1415−24.
10. Luo W, Zhou J, Yang X, Wu R, Liu H, Shao H, et al. A Chinese medical nutrition therapy diet accompanied by intermittent energy restriction alleviates type 2 diabetes by enhancing pancreatic islet function and regulating gut microbiota composition. *Food Res Int* 2022;**161**:111744.
11. Liu X, Du P, Xu J, Wang W, Zhang C. Therapeutic effects of intermittent fasting combined with SLBZS and prebiotics on STZ-HFD-induced type 2 diabetic mice. *Diabetes Metab Syndr Obes* 2024;**17**:4013−30.
12. Xu J, Fu C, Li T, Xia X, Zhang H, Wang X, et al. Protective effect of acorn (*Quercus liaotungensis* Koidz) on streptozotocin-damaged MIN6 cells and type 2 diabetic rats *via* p38 MAPK/Nrf2/HO-1 pathway. *J Ethnopharmacol* 2021;**266**:113444.
13. Li H, Zhang X, Wang F, Zhou L, Yin Z, Fan J, et al. MicroRNA-21 lowers blood pressure in spontaneous hypertensive rats by upregulating mitochondrial translation. *Circulation* 2016;**134**:734−51.
14. Tan Y, Li M, Li H, Guo Y, Zhang B, Wu G, et al. Cardiac urea cycle activation by time-restricted feeding protects against pressure overload-induced heart failure. *Adv Sci* 2024;**11**:e2407677.
15. Chen A, Lan Z, Li L, Xie L, Liu X, Yang X, et al. Sodium-glucose cotransporter 2 inhibitor canagliflozin alleviates vascular calcification

through suppression of nucleotide-binding domain, leucine-rich-containing family, pyrin domain-containing-3 inflammasome. *Cardiovasc Res* 2023;**119**:2368−81.
16. Wu T, Hu E, Xu S, Chen M, Guo P, Dai Z, et al. clusterProfiler 4.0: a universal enrichment tool for interpreting omics data. *Innovation* 2021;**2**:100141.
17. Szklarczyk D, Gable AL, Lyon D, Junge A, Wyder S, Huerta-Cepas J, et al. STRING v11: protein−protein association networks with increased coverage, supporting functional discovery in genome-wide experimental datasets. *Nucleic Acids Res* 2019;**47**:D607−13.
18. Xu HY, Tang XL, Li PF, Zhang DM, Ta G, Lu J, et al. Evaluating salidroside as a therapeutic agent for vascular calcification using network pharmacology and experimental rat models. *J Vis Exp* 2025; (215). Available from: https://doi.org/10.3791/67728.
19. Kee HJ, Cho S-N, Kim GR, Choi SY, Ryu Y, Kim IK, et al. Gallic acid inhibits vascular calcification through the blockade of BMP2-Smad1/5/8 signaling pathway. *Vasc Pharmacol* 2014;**63**:71−8.
20. Zhang P, Li Y, Du Y, Li G, Wang L, Zhou F. Resveratrol ameliorated vascular calcification by regulating Sirt-1 and Nrf2. *Transplant Proc* 2016;**48**:3378−86.
21. Ji R, Sun H, Peng J, Ma X, Bao L, Fu Y, et al. Rosmarinic acid exerts an antagonistic effect on vascular calcification by regulating the Nrf2 signalling pathway. *Free Radic Res* 2019;**53**:187−97.
22. Su R, Jin X, Zhao W, Wu X, Zhai F, Li Z. Rutin ameliorates the promotion effect of fine particulate matter on vascular calcification in calcifying vascular cells and ApoE$^{-/-}$ mice. *Ecotoxicol Environ Saf* 2022;**234**:113410.
23. Yu X, Xu L, Su C, Wang C, Wang Z, Wang Y, et al. Luteolin protects against vascular calcification by modulating SIRT1/CXCR4 signaling pathway and promoting autophagy. *AAPS J* 2024;**26**:111.
24. Chen C, Li Y, Lu H, Liu K, Jiang W, Zhang Z, et al. Curcumin attenuates vascular calcification *via* the exosomal miR-92b-3p/KLF4 axis. *Exp Biol Med (Maywood, NJ)* 2022;**247**:1420−32.
25. Tang F, Wu X, Wang T, Wang P, Li R, Zhang H, et al. Tanshinone II A attenuates atherosclerotic calcification in rat model by inhibition of oxidative stress. *Vasc Pharmacol* 2007;**46**:427−38.
26. Gunning PW, Hardeman EC. Tropomyosins. *Curr Biol* 2017;**27**: R8−13.
27. Huang H, Huang X, Luo S, Zhang H, Hu F, Chen R, et al. The microRNA MiR-29c alleviates renal fibrosis *via* TPM1-mediated suppression of the Wnt/β-catenin pathway. *Front Physiol* 2020;**11**:331.
28. Yang PY, Ho DCY, Chen SH, Hsieh PL, Liao YW, Tsai LL, et al. Down-regulation of miR-29c promotes the progression of oral submucous fibrosis through targeting tropomyosin-1. *J Formos Med Assoc* 2022;**121**:1117−22.
29. Wang Ss, Wang C, Chen H. MicroRNAs are critical in regulating smooth muscle cell mineralization and apoptosis during vascular calcification. *J Cell Mol Med* 2020;**24**:13564−72.
30. Jie P, Wu Y, Song C, Cheng Y, Liu Y, Chen K. Mechanism of Nrf2/miR338-3p/TRAP-1 pathway involved in hyperactivation of synovial fibroblasts in patients with osteoarthritis. *Heliyon* 2023;**9**: e21412.
31. Torella D, Iaconetti C, Tarallo R, Marino F, Giurato G, Veneziano C, et al. miRNA regulation of the hyperproliferative phenotype of vascular smooth muscle cells in diabetes. *Diabetes* 2018;**67**:2554−68.
32. Shen Z, Xu X, Lv L, Dai H, Chen J, Chen B. miR-21 overexpression promotes esophageal squamous cell carcinoma invasion and migration by repressing tropomyosin 1. *Gastroenterol Res Pract* 2020;**2020**:6478653.
33. Zhu S, Si ML, Wu H, Mo YY. MicroRNA-21 targets the tumor suppressor gene tropomyosin 1 (TPM1). *J Biol Chem* 2007;**282**:14328−36.
34. Lv L, Huang F, Mao H, Li M, Li X, Yang M, et al. MicroRNA-21 is overexpressed in renal cell carcinoma. *Int J Biol Markers* 2013;**28**:201−7.
35. Baker AH. MicroRNA 21 "shapes" vascular smooth muscle behavior through regulating tropomyosin 1. *Arterioscler Thromb Vasc Biol* 2011;**31**:1941−2.
36. Yahagi K, Kolodgie FD, Lutter C, Mori H, Romero ME, Finn AV, et al. ATVB in focus series on "Vascular Calcification in Diabetes". *Arterioscler Thromb Vasc Biol* 2017;**37**:191−204.
37. Yang HR, Song SS, Yi XL, Yu J, Xu CM. Research progress in prevention and treatment of vascular calcification with traditional Chinese medicine. *China J Chin Mater Med* 2024;**49**:4031−43.
38. Zhang J, Chen Y, Zhong Y, Wang Y, Huang H, Xu W, et al. Intermittent fasting and cardiovascular health: a circadian rhythm-based approach. *Sci Bull* 2025;**70**:2377−89.
39. Grajower MM, Horne BD. Clinical management of intermittent fasting in patients with diabetes mellitus. *Nutrients* 2019;**11**:873.
40. Zambuzzi WF, Ferreira MR, Wang Z, Peppelenbosch MP. A biochemical view on intermittent fasting's effects on human physiology-not always a beneficial strategy. *Biology* 2025;**14**:669.
41. Wang Y, Feng C, Yu B, Wang J, Chen W, Song C, et al. Enhanced effects of intermittent fasting by magnetic fields in severe diabetes. *Research (Washington, DC)* 2024;**7**:468.
42. Zhang L, Yao J, Yao Y, Boström KI. Contributions of the endothelium to vascular calcification. *Front Cell Dev Biol* 2021;**9**:620882.
43. Chen NX, Duan D, O'Neill KD, Moe SM. High glucose increases the expression of Cbfa1 and BMP-2 and enhances the calcification of vascular smooth muscle cells. *Nephrol Dial Transplant* 2006;**21**: 3435−42.
44. Sekaran S, Vimalraj S, Thangavelu L. The physiological and pathological role of tissue nonspecific alkaline phosphatase beyond mineralization. *Biomolecules* 2021;**11**:1564.
45. Villa-Bellosta R, Egido J. Phosphate, pyrophosphate, and vascular calcification: a question of balance. *Eur Heart J* 2017;**38**:1801−4.
46. Villa-Bellosta R. Vascular calcification: key roles of phosphate and pyrophosphate. *Int J Mol Sci* 2021;**22**:13536.
47. Dong Z, Chen Y. Transcriptomics: advances and approaches. *Sci China Life Sci* 2013;**56**:960−7.
48. Cao G, Xuan X, Hu J, Zhang R, Jin H, Dong H. How vascular smooth muscle cell phenotype switching contributes to vascular disease. *Cell Commun Signal* 2022;**20**:180.
49. Guo Y, Yang X, He J, Liu J, Yang S, Dong H. Important roles of the Ca^{2+}-sensing receptor in vascular health and disease. *Life Sci* 2018; **209**:217−27.
50. Xu S, Wang F, Mai P, Peng Y, Shu X, Nie R, et al. Mechanism analysis of vascular calcification based on fluid dynamics. *Diagnostics (Basel, Switzerland)* 2023;**13**:2632.
51. Girjes AA, Keriakous D, Hayward IP, Campbell GR, Campbell JH. Cloning of genes differentially regulated during change in vascular smooth muscle phenotype. *FEBS Lett* 2001;**509**:341−2.
52. Gagat M, Zielińska W, Mikołajczyk K, Zabrzyński J, Krajewski A, Klimaszewska-Wiśniewska A, et al. CRISPR-based activation of endogenous expression of TPM1 inhibits inflammatory response of primary human coronary artery endothelial and smooth muscle cells induced by recombinant human tumor necrosis factor α. *Front Cell Dev Biol* 2021;**9**:668032.
53. Afonso-Grunz F, Müller S. Principles of miRNA−mRNA interactions: beyond sequence complementarity. *Cell Mol Life Sci* 2015;**72**:3127−41.
54. Qin X, Ding R, Lu H, Zhang W, Wei S, Ji B, et al. Identification of pivotal genes and regulatory networks associated with atherosclerotic carotid artery stenosis based on comprehensive bioinformatics analysis and machine learning. *Front Pharmacol* 2024; **15**:1364160.
55. Zhao K, Zeng L, Cai Z, Liu M, Sun T, Li Z, et al. RNA sequencing-based identification of the regulatory mechanism of microRNAs, transcription factors, and corresponding target genes involved in vascular dementia. *Front Neurosci* 2022;**16**:917489.
56. Geng Z, Yu Y, Li Z, Ma L, Zhu S, Liang Y, et al. miR-21 promotes osseointegration and mineralization through enhancing both osteogenic and osteoclastic expression. *Mater Sci Eng C Mater Biol Appl* 2020;**111**:110785.
57. Sikora M, Śmieszek A, Pielok A, Marycz K. MiR-21-5p regulates the dynamic of mitochondria network and rejuvenates the senile phenotype of bone marrow stromal cells (BMSCs) isolated from osteoporotic SAM/P6 mice. *Stem Cell Res Ther* 2023;**14**:54.
58. Wang M, Li W, Chang GQ, Ye CS, Ou JS, Li XX, et al. MicroRNA-21 regulates vascular smooth muscle cell function *via* targeting

tropomyosin 1 in arteriosclerosis obliterans of lower extremities. *Arterioscler Thromb Vasc Biol* 2011;**31**:2044−53.
59. Jia S, Ma WD, Zhang CY, Zhang Y, Yao ZH, Quan XH, et al. Tanshinone IIA attenuates high glucose induced human VSMC proliferation and migration through miR-21-5p-mediated tropomyosin 1 downregulation. *Arch Biochem Biophys* 2019;**677**:108154.
60. Gunning P, O'Neill G, Hardeman E. Tropomyosin-based regulation of the actin cytoskeleton in time and space. *Physiol Rev* 2008;**88**: 1−35.
61. Hu S, Grobe H, Guo Z, Wang YH, Doss BL, Pan M, et al. Reciprocal regulation of actomyosin organization and contractility in nonmuscle cells by tropomyosins and alpha-actinins. *Mol Biol Cell* 2019;**30**: 2025−36.
62. O'Neill GM, Stehn J, Gunning PW. Tropomyosins as interpreters of the signalling environment to regulate the local cytoskeleton. *Semin Cancer Biol* 2008;**18**:35−44.
63. Prunotto M, Bruschi M, Gunning P, Gabbiani G, Weibel F, Ghiggeri GM, et al. Stable incorporation of α-smooth muscle actin into stress fibers is dependent on specific tropomyosin isoforms. *Cytoskeleton* 2015;**72**:257−67.
64. Dai B, Li H, Fan J, Zhao Y, Yin Z, Nie X, et al. MiR-21 protected against diabetic cardiomyopathy induced diastolic dysfunction by targeting gelsolin. *Cardiovasc Diabetol* 2018;**17**:123.
65. Chiou TT, Liao SC, Kao YY, Lee WC, Lee YT, Ng HY, et al. Gelsolin and progression of aortic arch calcification in chronic hemodialysis patients. *Int J Med Sci* 2016;**13**:92−8.